Rapid CAR Screening and circRNA-driven CAR-NK Cells for Persistent Shed-resistant Immunotherapy

Joo-Yoon Chung[1,2,†], Jisu Hong[3,†], Su-Min Yee[1], Hye Won Lim[4], Dahye Lee[5], Sangwon Yoon[6], Seung-Hwan Lee[7,8], Yujin Jung[3], Seung hun Shin[1,9], Song Cheol Kim[10], Chang-Han Lee[3,4,5,11,12,*], Mihue Jang[1,2,13*]

[1]*Medicinal Materials Research Center, Biomedical Research Division, Korea Institute of Science and Technology (KIST), Seoul 02792, Republic of Korea*

[2]*KHU-KIST Department of Converging Science and Technology, Kyung Hee University, Seoul 02447, Republic of Korea*

[3]*Department of Biomedical Sciences, Seoul National University College of Medicine, Seoul 03080, Republic of Korea*

[4]*Cancer Research Institute, Seoul National University College of Medicine, Seoul 03080, South Korea*

[5]*Department of Pharmacology, Seoul National University College of Medicine, Seoul 03080, Republic of Korea*

[6]*Corporate Research & Development Center, UCI Therapeutics, Seoul 04784, Republic of Korea*

[7]*Department of Biochemistry, Microbiology and Immunology, Faculty of Medicine, University of Ottawa, Ottawa, Ontario K1N 6N5, Canada*

[8]*Ottawa Institute of Systems Biology, Faculty of Medicine and Centre for Infection, Immunity, and Inflammation, Faculty of Medicine, University of Ottawa, Ontario K1N 6N5, Canada*

[9]*Medicinal Materials Research Center, Biomedical Research Division, Korea Institute of Science and Technology, Seoul 02792, Republic of Korea*

[10]*Division of Hepato-Biliary and Pancreatic Surgery, Department of Surgery, University of Ulsan College of Medicine, Asan Medical Center 05505, Seoul, Republic of Korea*

[11]*BK21 FOUR Biomedical Science Project, Seoul National University College of Medicine, Seoul 03080, Republic of Korea*

[12]*Wide River Institute of Immunology, Seoul National University, Hongcheon 25159, Republic of Korea*

[13]*Division of Bio-Medical Science and Technology, KIST School, University of Science and Technology (UST), Seoul 02792, Republic of Korea*

[†]These authors contributed equally to this work.

KEYWORDS

Pancreatic cancer; Tumor microenvironment; Shed mesothelin, mRNA; mRNA-CAR-NK; Circular RNA;

*Corresponding author

Mihue Jang, Ph.D.

Tel: +82-2-958-6618; fax: +82-2-958-5909, e-mail: mihue@kist.re.kr

Chang-Han Lee, Ph.D

Tel: +82-2-740-8278; email: chlee-antibody@snu.ac.kr

ABSTRACT

Chimeric antigen receptor (CAR)-based therapeutics offer great potential against cancer and autoimmune diseases. This study presents a high-throughput mRNA-based platform to rapidly screen and optimize CAR-NK cells targeting shed-resistant membrane-proximal epitopes of mesothelin (MSLN)—an antigen frequently overexpressed in solid tumors. Using a yeast surface-display library, we identified single-chain variable fragments that selectively bind membrane-immobilized mature MSLN, minimizing inhibition by soluble MSLN (solMSLN) and enhancing cell-cell avidity. Linear mRNA (linRNA) encoding CAR was electroporated into human primary NK cells for live-cell phenotyping screening of antigen-specific cytotoxicity. Final optimization included co-stimulatory domain (OX40ζ) and cytokine (IL21) co-transfection. The finalized circular mRNA (circRNA)-based CAR-MS10-NK cells exhibited prolonged CAR and superior anti-tumor activities in MSLN-positive models, including solMSLN-secreting pancreatic tumors. *In vivo*, circCAR-MS10-NK cells significantly reduced tumor burden, outperforming lentivirus-based CAR-NK counterparts in both potency and manufacturability. This platform enables rapid non-viral CAR design and functional screening, for the scalable cost-effective development of shed-resistant antigen-targeting immunotherapies.

1. Introduction

Natural killer (NK) cells are innate immune effectors that exert rapid and potent cytotoxicity against cancer and virus-infected cells without prior sensitization, making them a promising platform for chimeric antigen receptor (CAR)-based therapies [1]. CAR-NK cells integrate the antigen specificity of CAR constructs with the intrinsic cytotoxic mechanisms of NK cells, enhancing overall anti-tumor efficacy [2]. Compared to CAR-T cells, CAR-NK cells offer several advantages in therapies, including a lower risk of graft-versus-host disease (GVHD) and cytokine release syndrome (CRS), with the potential for off-the-shelf, allogeneic applications [3-6]. NK cells can be obtained from various sources, such as umbilical cord blood, peripheral blood, NK cell lines, and induced pluripotent stem cells (iPSC), enabling scalable manufacturing [3, 7]. However, the manufacturing of CAR-NK cells is limited by poor gene-delivery efficiency, scalability issues, and the high labor and time costs associated with viral transduction methods [8, 9]. Lentiviral or retroviral vectors are standard agents for CAR gene delivery, often using a vesicular stomatitis virus glycoprotein (VSV-G) envelope that primarily targets cells expressing the low-density lipoprotein receptor (LDL-R). Because NK cells typically express low or undetectable levels of LDL-R, the transduction efficiency of VSV-G–pseudotyped vectors is greatly impaired [10, 11]. Alternative envelope proteins, such as the baboon endogenous retrovirus (BaEV) envelope, have improved NK-cell transduction by exploiting receptors such as ASCT-1 and ASCT-2[12, 13], yet large-scale viral manufacturing and stability issues limit their clinical feasibility[14]. This highlights a growing demand for rapid non-viral gene delivery approaches for efficient functional optimization of CAR constructs.

Mesothelin (MSLN) is as a promising target for cancer immunotherapy due to its high expression in various malignancies, including mesothelioma, ovarian cancer, pancreatic adenocarcinoma, gastric adenocarcinoma, and triple-negative breast cancer, while showing

limited expression in normal tissues [15-17]. Elevated MSLN levels often correlate with aggressive clinical features and poor prognosis in both pancreatic and colorectal cancer, suggesting a role in immune evasion and tumor progression [18-20]. Despite their promise, MSLN-targeted strategies are hampered by “shedding,” in which the MSLN ectodomain is proteolytically cleaved and released as soluble MSLN (solMSLN) [21, 22]. The soluble form can sequester CAR molecules, blocking effective tumor-cell engagement and reducing CAR-mediated cytotoxicity [23].

The performance of CAR-T and CAR-NK cell-based therapies is closely linked to the affinity, epitope specificity, and membrane proximity of the selected antibody or single-chain variable fragment (scFv) [24-26]. Reformatted antibodies originally designed for non-CAR applications often underperform, necessitating iterative testing to ensure favorable antigen recognition, immune-synapse formation, and signaling [27, 28]. Addressing these issues typically requires the functional evaluation of each antibody in the CAR format—a time-consuming and labor-intensive process that relies on viral vector-based CAR-T/NK cell generation [27-29].

Given these manufacturing and biological challenges, we aimed to develop novel anti-MSLN antibodies that retain binding capacity in the presence of shed MSLN and are optimized for CAR functionality in NK cells. To accelerate CAR discovery, we established an innovative mRNA-based platform that relies on simple electroporation instead of viral transduction for high-throughput phenotypic screening of diverse scFv, co-stimulatory domain, and cytokine traits in NK cells. We assessed the effects of circular mRNA (circRNA) encoding CAR expression on protein production and superior anti-tumor activity compared to linear mRNA (linRNA). Using this platform, we identified and refined CAR constructs that effectively target shed-resistant MSLN epitopes in solid tumors, providing a promising framework for developing targeted CAR-NK cell-based immunotherapies.

2. Results and discussion

2.1. Selective scFv screening against mature MSLN (matMSLN) using yeast display library system)

To generate high-affinity antibodies against matMSLN (residues 296–606), 6-week-old BALB/c mice were immunized intraperitoneally with recombinant matMSLN protein **(Figs. 1, 2A and S1).** Upon reaching a serum antibody titer of 10% inhibitory concentration (IC_{10}) 1:100,000 **(Fig. S2**), variable heavy (VH) and light (VL) chain genes were amplified from the spleen and bone marrow of sacrificed immunized mice, fused to their respective constant domains, and transformed into *Saccharomyces cerevisiae* strains JAR200 (MATa) and YVH10 (MATα) to construct heavy-chain (HC) and light-chain (LC) Fab libraries. Mating the HC and LC yeast libraries [30, 31], yielded a combinatorial Fab repertoire ($> 4 \times 10^7$) **(Fig. S3A and Table S1).** Flow cytometric selection of clones with high antigen-binding activity, subsequent cell-based panning on $MSLN^+$ and $MSLN^-$ AsPC-1 cells narrowed the candidates to 96 unique Fab clones **(Figs. S3B and S4)**. Most antibody candidates exhibited strong matMSLN binding but negligible affinity for solMSLN (residues 296–592), indicating a favorable selectivity that may reduce interference from shed MSLN **(Fig. 2A, B)** [23, 32, 33].

Based on their binding profiles and expression levels, seven antibody clones—CLMS10, CLMS20, CLMS32, CLMS36, CLMS76, CLMS88, and CLMS95—were selected for further analysis **(Fig. 2B)**. After producing recombinant scFvs [34, 35], their binding activities to both matMSLN and solMSLN were evaluated by ELISA **(Fig. 2C, D)**. Except for CLMS32 and CLMS36, all clones showed selective binding to matMSLN ($IC_{50} = 1.7 \pm 0.1$–151.1 ± 33.3 nM; **Table S2**) over solMSLN. Notably, CLMS10 demonstrated high affinity for matMSLN ($IC_{50} = 18.6 \pm 1.1$ nM), while exhibiting minimal binding to solMSLN ($IC_{50} > 1$ μM). Surface plasmon resonance (SPR) confirmed that the affinity of CLMS10 for

matMSLN was 8.22 ± 0.40 nM (**Fig. S5**). All scFvs, except CLMS20 and CLMS88, specifically bound to MSLN-positive K562 cells, with IC_{50} values from a few nM to several hundred nM, while showing negligible binding to MSLN-negative K562 cells **(Fig. 2E, F and Table S3)**. These results indicate that our anti-MSLN antibodies selectively recognize membrane-bound MSLN on the cell surface.

To further define the epitope of antibody candidates, we performed a competitive ELISA using reference antibodies with well-characterized binding sites: SS1, which targets domain I (residues E296–L398) [36], and 15B6, which binds the C-terminal region (residues Y594–L605)[23]. CLMS10, CLMS32, CLMS36, CLMS76, and CLMS95 competed for antigen binding, suggesting that they either share overlapping epitopes or exhibit steric hindrance that prevents simultaneous binding **(Fig. 2G)**. Notably, CLMS10 exhibited weak binding to solMSLN **(Fig. 2D)**, implying that its epitope is localized near the C-terminus of domain III— known to be susceptible to proteolytic shedding **(Fig. 2H)**. Collectively, these findings suggest that the epitopes of CLMS10, CLMS32, CLMS36, CLMS76, and CLMS95 are clustered near the C-terminal region of domain III, supporting their therapeutic potential as shed-resistant antibodies **(Fig. 2H)**.

2.2. High-throughput live-cell screening of functional scFvs using linRNA-based CAR-NK (linCAR-NK) cell platform

To evaluate the performance of the scFv candidates in terms of CAR constructs, we established a rapid CAR-NK generation platform using linRNA-based electroporation. This provides a simple and time-efficient approach for live high-throughput functional screening (**Fig. 1 and 3A**). Each scFv-containing CAR construct was synthesized as linRNA via *in vitro* transcription. The quality of the synthesized linRNA was validated by agarose gel

electrophoresis (AGE) and purity assessment (**Fig. S6A**). Primary NK cells were electroporated with linRNA, and CAR expression and cell viability were assessed in a time- and dose-dependent manner. For instance, CAR-SS1-NK cells exhibited over 87% CAR expression at 1 µg linRNA/10^6 cells, with detectable expression persisting for up to 7 d, albeit at a reduced level **(Fig. S6B, C)**. Following linRNA electroporation, flow cytometry confirmed CAR and GFP expression across all clones, with GFP co-expressed via a P2A linker. CAR expression levels varied among constructs-as CAR was detected by staining with PE-conjugated streptavidin and biotinylated MSLN extracellular domain proteins **(Figs. S6D and S7)**. Cell viability was largely consistent across clones (**Fig. S6E)**.

We established a high-throughput live-cell screening platform to assess the cytotoxic function of linCAR-NK cells against an MSLN-overexpressing pancreatic cancer cell line (Capan-2). Real-time cancer cell death by linCAR-NK cells was monitored by tracking Caspase-3/7 activation during live co-culture **(Fig. 3B, C and Fig. S8A)**. CAR-SS1-NK and CAR-15B6 NK cells were used as controls. Notably, CAR-MS10-NK cells caused a significant increase in cancer cell death, as evidenced by a 1.5-fold elevation in caspase-3/7-positive Capan-2 cells compared to mock-NK cells. In parallel, a luciferase-based cytotoxicity assay showed that CAR-MS-10-NK cells achieved the strongest killing efficacy against both Capan-2-Luc and SK-OV-3-Luc cells, expressing different MSLN levels **(Fig. S8B, C)**. We assessed the sensitivity of each CAR-NK construct to solMSLN-mediated inhibition. In co-culture with solMSLN, CAR-SS1-NK, CAR-MS32-NK, and CAR-MS36-NK cells exhibited a dose-dependent reduction in killing activity. In contrast, CAR-MS10-NK, CAR-15B6-NK, and CAR-MS20-NK cells maintained their cytotoxicity, indicating resistance to solMSLN-mediated inhibition **(Fig. 3D)**. The expression of CD107a—a marker of degranulation—was unaffected by solMSLN treatment in CAR-MS10-NK, CAR-MS-20-NK, and CAR-15B6-NK cells activated with matMSLN, further supporting their shed-

resistant profiles **(Fig. 3E)**. We examined the extent of trogocytosis associated with impaired CAR function and NK-mediated fratricide [37, 38] in linCAR-NK cells [37, 38]. Remarkably, CAR-MS10-NK exhibited significantly reduced trogocytosis compared to CAR-SS1-NK cells **(Fig. S8D).** Furthermore, CAR-MS10-NK cells exhibited the highest cell avidity among all tested CAR constructs, suggesting the formation of a robust immunological synapse **(Fig. 3F)** [39]. To validate these findings in a more clinically relevant system, we introduced the scFvs into lentivirus-based CAR constructs and transduced these in primary NK cells. Functional assays revealed similar cytotoxicity patterns as seen with linCAR-NK cells, with CAR-MS10-NK cells once again showing a statistically significant 22.57 % higher killing rate against Capan-2 cells compared to CAR-SS1- and CAR-15B6-transduced cells **(Fig. 3G and S9A)**. We evaluated whether this functional trend persisted across immune cell types such as linCAR-T cells. In cytotoxicity assays against Capan-2-Luc cells, linCAR-15B6-T cells showed comparable efficacy to linCAR-MS10-T and linCAR-SS1-T cells **(Fig. S9B–F).** CAR-MS20-T cells showed limited activity, consistent with the NK cell results, suggesting that the functional impact of scFvs may vary depending on the immune effector cell type.

Finally, *in silico* docking analysis showed that CLMS10 interacts with both matMSLN and solMSLN at an epitope overlapping the proteolytic cleavage site **(Fig. 3H).** This localization may account for the observed resistance to solMSLN-mediated inhibition and its enhanced cytotoxicity. Among the scFvs, CLMS10 emerged as the most promising for CAR engineering, providing robust cytotoxicity and shed-resistance in CAR-NK and CAR-T cell-based platforms. Collectively, our linRNA-based screening platform offers an efficient functional approach for discovering and optimizing clinically relevant MSLN-targeting CARs.

2.3. linRNA-driven screening for optimized CAR architecture and cytokine co-expression

We selected CAR-MS10 for further analysis. We employed the linRNA-based system to screen various combinations of transmembrane and costimulatory domains. Specifically, CD8 and NKG2D were chosen as transmembrane domains (TMD_{CD8} and TMD_{NKG2D}), and four CAR variants were designed: TMD_{CD8}–4-1BB–CD3ζ (4-1BBζ), TMD_{CD8}–OX40–CD3ζ (OX40ζ), TMD_{NKG2D}–DAP10–DAP12 (DAP10/12), and TMD_{NKG2D}–2B4–CD3ζ (2B4ζ) **(Fig. 4a).**

The cytotoxic potential of the CAR variants against Capan-2-Luc cells was evaluated using a luciferase-based killing assay. Among the variants, the CAR-MS10-OX40ζ construct exhibited the strongest cytotoxicity, followed by CAR-MS10-4-1BBζ **(Fig. 4B and S10A)**. A detailed analysis of the functional activities across the 4-1BBζ and OX40ζ constructs showed that consistent with the cytotoxicity data, CAR-MS10-OX40ζ exhibited a significant increase in CD107a activation compared to the prototype CAR-MS10-41BBζ, accompanied by elevated secretion of IFN-γ **(Fig. 4C, D)**. Remarkably, CAR-MS10-OX40ζ also enhanced metabolic activity when stimulated with MSLN recombinant protein, showing greater basal and maximal respiration than the prototype **(Fig. 4E, F)**. To further investigate the underlying signaling pathways in OX40ζ-mediated CAR activation, CAR-MS10-OX40ζ-NK cells were stimulated using a MSLN recombinant protein and analyzed via western blotting **(Fig. 4G).** The OX40ζ group demonstrated stronger phosphorylation of PLCγ and extracellular signal-regulated kinase (ERK), key downstream molecules of CD3ζ signaling [40, 41], compared to the 4-1BBζ group. Collectively, these results identify OX40ζ as the optimal intracellular domain configuration for CAR-MS10, enhancing both effector function and signaling capacity.

We co-transfected cytokine-encoding linRNA in CAR-MS10-OX40ζ to enhance its

cytotoxicity and functionality. Cytokines play a pivotal role in modulating NK cell activity, proliferation, and persistence [42-44]. Based on their well-characterized functions, we selected interleukin IL2, IL15, and IL21 to reinforce NK cell effector function and longevity. The synergistic effects of the selected cytokines were evaluated in CAR-MS10-NK cells, generated by co-electroporating CAR-MS10-OX40ζ linRNA with linRNAs encoding each cytokine **(Fig. 4H and S10B, C).** Among the various cytokine combinations, IL21–CAR-MS10-OX40ζ-co-expressing NK cells demonstrated the strongest anti-tumor activity against Capan-2 Luc cells, along with significantly enhanced CD107a expression **(Fig. 4I, J)**. Taken together, the linRNA-based approach demonstrated that the IL-21–CAR-MS10-OX40ζ configuration empowers NK cells with superior cytotoxicity and functional activity.

2.4. circRNA-based CAR-NK exhibited superior cytotoxicity with prolonged CAR expression

To address the transient nature of linRNA expression in mRNA-based cell therapies, we explored the use of circRNA for prolonging CAR expression. circRNA has previously been used to prolong transgene expression and offers improved structural stability and translational efficiency compared to linRNA [45-47]. We monitored CAR expression and cell viability over time in CAR-NK cells generated using either linRNA or circRNA **(Fig. 5A)**. Notably, circCAR-NK cells exhibited significantly prolonged and sustained CAR expression, with high fluorescence intensity maintained for up to 5 d **(Fig. 5 B, C)**. In contrast, there was no notable difference in viability between linRNA and circRNA-transfected cells **(Fig. 5D)**. We evaluated the persistence of cytotoxicity using a serial killing assay, where CAR-NK cells were challenged with fresh cancer cells over five rounds **(Fig. 5E)**. As expected, circCAR-NK cells maintained superior activity, though a gradual decline was observed over time **(Fig.**

5F). circCAR-NK cells exhibited robust IFN-γ secretion, suggesting a correlation between prolonged CAR expression and sustained effector function **(Fig. 5G)**. circCAR-MS10-NK retained strong cytotoxic activity even under solMSLN-shedding conditions, indicating resistance to solMSLN-decoy effects **(Fig. 5H)**. In contrast, circCAR-SS1-NK cells showed limited cytotoxicity and a marked reduction in IFN-γ secretion in the presence of solMSLN, highlighting the importance of target epitope selection and construct design **(Fig. 5I)**. Together, these findings underscore the superior performance of circCAR-NK cells over their linRNA counterparts, demonstrating enhanced CAR expression, prolonged cytotoxicity, and greater functional resilience under repeated tumor challenge and antigen-shedding stress.

2.5. circCAR-MS10-NK cells show potent anti-tumor activity in solMSLN-shedding models *in vitro* and *in vivo*

The pancreatic tumor microenvironment (TME) is highly immunosuppressive, characterized by a dense extracellular matrix and abundant TGFβ signaling, primarily originating from cancer-associated fibroblasts (CAFs). This milieu impairs NK cell function and greatly challenges the efficacy of immunotherapies [48-50]. Recent studies demonstrated that anti-mesothelin antibodies not only target tumor cells but also disrupt antigen-presenting CAFs, reshaping the TME and enhancing immune responses [51]. However, the therapeutic efficacy of MSLN-targeted CAR-T therapies is undermined by the decoy effect of solMSLN-mediated antigen shedding, impeding CAR-T cell activity [23]. To address the suppression of CAR-T cell function induced by solMSLN under physiologically relevant conditions, we established an *in vitro* cancer–CAF co-culture model to mimic the TME. Interestingly, we found that the presence of human primary pulmonary fibroblast (HPPF) or CAFs derived from patients with pancreatic cancer significantly accelerated the secretion of solMSLN compared to cancer

cells alone **(Fig. 6A, B and S11A, B)**.

Based on the observed increase in solMSLN secretion in the presence of CAFs, we further assessed the therapeutic efficacy of CAR-NK cells under CAF-mediated shedding inhibition using real-time live-cell imaging **(Fig. 6C and S11C)**. The CAF-induced elevation in solMSLN levels significantly reduced cancer cell death in the circCAR-SS1-NK cell-treated group. In contrast, circCAR-MS10-NK cells maintained their cytotoxic efficacy despite solMSLN shedding. Surprisingly, strong MSLN expression was associated with advanced cancer progression, as evidenced by CLMS10-IgG staining in pancreatic tumor tissues, reinforcing MSLN as a therapeutically actionable target **(Fig. 6D)**. We established an in vivo intraperitoneal metastatic tumor model that mimics the TME [3, 23], including solMSLN shedding, by co-injecting Capan-2-Luc tumor cells and CAFs into NSG mice treated with various CAR-NK platforms: linCAR-NK cells expressing CAR-SS1, CAR-15B6, or CAR-MS10; circCAR-MS10-NK cells; and $_{LV}$CAR-MS10-NK cells **(Fig. 6E)**. To enhance NK cell function and persistence, IL-21 linRNA was co-electroporated into all mRNA-based CAR-NK groups, but not into the lentivirus-based groups. Remarkably, both the circRNA-based and lentivirus-based CAR-MS10-NK groups demonstrated significant tumor regression compared with the mock group **(Fig. 6F-I)**. Unexpectedly, circCAR-MS10-NK cells outperformed showed greater anticancer activity than $_{LV}$CAR-MS10-NK cells. In contrast, the linCAR-NK cells induced a modest reduction in tumor size compared to the mock group, though not significantly so. These findings demonstrate that optimized circCAR-MS10-NK cells retain antitimor efficacy under TME-mimicking conditions and elevated solMSLN levels, supporting the potential applicability of the non-viral CAR-NK platform for treating solid tumors.CAR-based immunotherapy for solid tumors remains ineffective largely due to antigen loss, shedding, and the immunosuppressive TME, which impedes immune-cell infiltration and function.[52] In this study, we developed a comprehensive, non-viral strategy

for rapid CAR discovery and optimization, culminating in a shed-resistant MSLN-targeted CAR-NK cell-based system with persistent cytotoxicity. Our approach integrates rational antibody engineering, high-throughput mRNA-based functional screening, and circRNA technology to overcome the limitations of current solid tumor therapies. A principal obstacle in targeting MSLN is the shedding of the extracellular domain, which acts as a decoy receptor, sequestering CARs and diminishing cytotoxic potential [53, 54]. In this study, we generated a panel of MSLN-specific antibodies and demonstrated the performance of CLMS10 for binding membrane-proximal epitopes while displaying minimal affinity for solMSLN (**figure 2**). In contrast to SS1, the CLMS10-based CAR maintained strong cytotoxic activity even under high solMSLN concentrations, emphasizing the importance of epitope selection (**figure 2C–H, 3D–G**). Notably, these shed-resistant CARs demonstrated efficacy across both NK and T cells, indicating broad applicability across effector platforms.

A key innovation of our workflow is the use of high-throughput mRNA-based CAR screening of primary immune cells. Electroporation-based delivery bypasses the efficacy and safety constraints of viral transduction, particularly in NK cells, where viral uptake is limited.[55] This mRNA approach enabled rapid parallel testing of multiple scFv candidates, co-stimulatory domains, and cytokine co-delivery, accelerating the identification of functionally superior CARs [52, 56]. Among cytokine candidates, IL21 remarkably enhanced PI3K/Akt activation [43, 57]; triggering the expression of T-BET, EOMES, and CEBPD; enhancing NK cell anti-tumor function, survival, and metabolic fitness; and strengthening long-term anti-tumor efficacy [43, 58]. Notably, the combination of the OX40ζ signaling domain and IL21 co-delivery yielded potent antitumor effects, demonstrating the synergistic value of optimized intracellular signaling and transient cytokine support (**figure 4B–J**).

Another major advance is the application of circRNA for CAR expression in NK cells. Compared to linRNA, circRNA exhibited prolonged transcript stability and sustained CAR

expression, owing to its resistance to exonuclease degradation [59, 60]. circCAR-NK cells remained functionally active during serial tumor challenges, with cytotoxicity maintained despite repeated antigen exposure **(figure 5)**. This highlights the unique advantage of circRNA in bridging transient and durable CAR expression systems—combining the safety of RNA-based approaches with the persistence of integrating vectors.

In terms of translational relevance, we tested our platform in a CAF-rich tumor model—a setting characterized by dense stroma, high solMSLN levels, and immunosuppressive factors. While CAFs compromised the cytotoxicity of CAR-SS1-NK cells, circCAR-MS10-NK cells retained potent cytotoxicity (**figure 6A-C**). Human pancreatic tumor tissues showed high MSLN expression (**figure 6D**). In Capan-2/CAF xenografts, circCAR-MS10-NK cells achieved tumor regression, outperforming lentiviral CARs (**figure 6E-I**). These findings underscore the platform's shed-resistance and persistence under clinically relevant TME conditions.

Our RNA engineering strategy supports the development of off-the-shelf, allogeneic CAR-NK therapies. NK cells are inherently less prone to GVHD and CRS than T cells, providing a potential universal donor base [61-63]. Previous trials using HLA-mismatched cord blood-derived CAR-NK cells expressing IL15 have demonstrated safe and durable responses in patients [64]. By avoiding viral vectors, our mRNA and circRNA systems reduce manufacturing complexity, shorten production timelines, and enable rapid adaptation to new targets [65]. The transient expression profile of RNA further permits repeat dosing and modular CAR redesign, offering unmatched flexibility. Furthermore, recent advances in circRNA synthesis, particularly self-splicing intron-based circularization-have improved yield and scalability, facilitating broader application of this approach in cell therapy manufacturing [66-68]. While our shed-resistant circCAR-MS10-NK cells demonstrate strong potential in addressing antigen shedding and mitigating elements of the immunosuppressive tumor

microenvironment (TME), solid tumors such as pancreatic cancer remain highly refractory due to additional resistance mechanisms. These include antigen downregulation and the secretion of immunosuppressive factors like TGF-β within the dense stromal matrix [69-71]. Consequently, further studies are warranted to assess the long-term persistence, tumor trafficking, and safety of circRNA-engineered CAR-NK cells *in vivo*. Future therapeutic strategies may benefit from combining these cells with agents targeting complementary immune escape pathways, such as immune checkpoint inhibitors or TGF-β blockade, to enhance antitumor efficacy within the complex TME. Further investigation is needed to evaluate the long-term persistence, trafficking, and safety of circCAR-MS10-NK cells.

In conclusion, we propose a novel framework for generating shed-resistant, long-lasting CAR-NK therapies with enhanced cell-cell avidity against solid tumors. By integrating antibody engineering, rapid mRNA-based CAR discovery, and circRNA-mediated expression, we address key limitations of CAR-based therapies for solid tumors. The circCAR-MS10-NK system offers a potent, scalable, and clinically translatable solution for treating malignancies such as pancreatic cancer, effectively addressing issues related to antigen shedding and immunosuppressive TMEs that have previously impeded therapeutic success.

3. Conclusion

We have successfully developed shed-resistant circRNA engineered CAR-NK cells targeting membrane-proximal epitopes of MSLN, frequently overexpressed in solid tumors such as pancreatic cancers. Leveraging a high throughput mRNA-based screening platform, these CAR-NK cells were optimized with the OX40ζ co-stimulatory domain and IL21 co-delivery, resulting in enhanced metabolic activity, effector function, and persistence. Notably, circCAR-MS10-NK cells maintained potent cytotoxicity under TME mimicking conditions

enriched with CAF driven soluble MSLN shedding, outperforming their lentiviral counterparts in both potency and manufacturability. Consequently, our results suggest the potential of this non-viral, circRNA-based CAR-NK platform to overcome TME induced impairments and antigen-shedding barriers in CAR-NK cell mediated immunotherapy, offering a scalable and clinically translatable strategy for the effective treatment of solid tumors.

4. Materials and Methods

4.1. Yeast strains and culture conditions

S. cerevisiae JAR200 (MATa, GAL1-AGA1::KanM×4ura3D45, ura3–52 trp1 leu2D1 his3D200 pep4::HIS3 prb1D1.6R can1) and YVH10 (MATα, PDI::ADHII-PDI-Leu2 ura3-52 trp1 leu2D1 his3D200 pep4::HIS3 prb1D1.6p can1 GAL) were used to construct and screen the yeast surface-display Fab library. Both strains were kindly provided by Prof. Dane Wittrup (Massachusetts Institute of Technology, Cambridge, MA, USA). The haploid yeast library was maintained in SDCAA (6.7 g/L yeast nitrogen base, 5 g/L casamino acids, 14.7 g/L sodium citrate, 4.29 g/L citric acid monohydrate, and 20 g/L dextrose in deionized water) supplemented with either uracil (0.0002g/L) for JAR200 or tryptophan (0.0004g/L) for YVH10, while the diploid Fab library was maintained in SDCAA without additional supplements. The Fab surface display library was induced in 2× SGCAA medium (13.4 g/L yeast nitrogen base, 10 g/L casamino acids, 5.4 g/l Na_2HPO_4, 8.56 g/L $NaH_2PO_4 \cdot H_2O$, and 20 g/L galactose in deionized water) at a starting OD_{600} of 0.5, with incubation at 20°C and 160 rpm for 48 h.

4.2. Cell lines and culture

MSLN-positive AsPC-1, parental AsPC-1, MSLN-positive K562, and parental K562 cells were cultured in RPMI 1640 medium (Welgene, Gyeongsan, Republic of Korea) supplemented with 10% fetal bovine serum (FBS; Gibco, Waltham, MA, USA) and 1× penicillin-streptomycin (Gibco, USA). All cells were maintained at 37 °C in a humidified atmosphere containing 5% CO_2. The pancreatic cancer Capan-2 and ovarian cancer SK-OV-3 cell lines were obtained from the Korean Cell Line Bank (Seoul, Republic of Korea). Capan-2 cells were cultured in RPMI 1640 medium (Welgene) supplemented with 10% FBS (Welgene) and 1% antibiotic–antimycotic solution (Welgene). SK-OV-3 cells were cultured in McCoy's 5A medium (Gibco) supplemented with 10% FBS (Gibco) and 1% antibiotic-antimycotic (AA) solution (Welgene). HEK293T cells were obtained from American Type Culture Collection (ATCC; Manassas, VA, USA) and were maintained in Dulbecco's Modified Eagle Medium (DMEM; Welgene) supplemented with 10 % FBS (Welgene), 1 % AA solution (Welgene) and 10 mH HEPES. Primary pancreatic CAFs and HPPF were obtained from Asan Medical Center (Seoul, Republic of Korea) and ScienCell Research Laboratories (Carlsbad, CA, USA), respectively. Both CAFs and HPPFs were cultured in RPMI1640 medium (Welgene) supplemented with 10% FBS (Welgene) and 1% AA solution (Welgene), and 10 ng/mL fibroblast growth factor (FGF; PeproTech, Rocky Hill, NJ, USA). All cultures were maintained at 37 °C in a humidified incubator with 5 % CO_2.

4.3. Preparation of recombinant proteins

To express matMSLN (residues 296–606) and solMSLN (residues 296–592), both MSLN gene sequences (synthesized by Integrated DNA Technologies, Coralville, IA, USA) were cloned into the pcDNA3.4 mammalian expression vector via Gibson assembly. Protein expression was performed in Expi293 cells (Thermo Fisher Scientific, Waltham, MA, USA), and His-tagged MSLN proteins were purified by affinity chromatography using Ni-NTA

agarose resin (QIAGEN, Germantown, MD, USA). Following elution and buffer exchange, protein purity was confirmed by SDS-PAGE. Recombinant MSLN proteins were biotinylated using an EZ-Link™ Sulfo-NHS Biotinylation Kit (Thermo Fisher Scientific).

4.4. Mouse immunization

BALB/c mice (6 weeks old) were immunized biweekly via intraperitoneal injection of 50 μg MSLN-His protein mixed with aluminum hydroxide adjuvant [1:1 (v/v); Thermo Fisher Scientific]. Blood samples were collected weekly to monitor the immune response. Sera were separated by centrifugation and used to measure anti-MSLN antibody levels. For the ELISA, 100 ng matMSLN was coated onto the bottom of each well of 96-well MaxiSorp microplates (Thermo Fisher Scientific) and incubated overnight at 4 °C. After blocking with phosphate-buffered saline (PBS, pH 7.4) containing 3% bovine serum albumin (BSA; Sigma-Aldrich, St. Louis, MO, USA) for 1 hour at room temperature, the plates were washed three times with PBST phosphate-buffered saline (PBS, pH 7.4containing 0.05% Tween 20). Mouse sera were serially diluted 10-fold and incubated on the experimental plates for 1 hour at room temperature. After washing, horseradish peroxidase (HRP)-conjugated goat anti-Mouse IgG (H+L) secondary antibody (1:8,000; Cat. 31430, Invitrogen, Carlsbad, CA USA) was added and incubated for 1 hour. Following three additional washes, the plates were developed using 3,3′,5,5′-tetramethylbenzidine (TMB) substrate. The reaction was stopped by adding 2 M H_2SO_4, and absorbance was measured at 450 nm using an Infinite 200 PRO NanoQuant microplate reader (Tecan Trading AG, Männedorf, Switzerland).

4.5. Construction of the immune Fab library

Following the final immunization, mice were sacrificed, and mRNA was isolated from spleen

and bone marrow samples. The VH and VL genes were amplified from cDNA using a primer mixture **(Supplementary Table 1)**. Through overlapping PCR, each amplified VH and VL gene was fused to the CH1 and CL region, respectively. The resulting VH-CH1 fragment (4 μg) was co-transformed with the linearized pYDS-H vector into *S. cerevisiae* strain JAR200, while the VL-CL fragment was co-transformed with the linearized pYDS-K vector into *S. cerevisiae* strain YVH10. Homologous recombination facilitated by electroporation was used for both transformations. The resulting haploid HC library in JAR200 (MATa) and LC library in YVH10 (MATα) were cultured for 15 h at 30 °C and 160 rpm in 200 mL SDCAA medium supplemented with uracil (for JAR200) or tryptophan (for YVH10), reaching an OD□□□ of ~5 in the late exponential phase. For mating, equal volumes (OD□□□ = 100) of the HC and LC library cells were mixed thoroughly by vortexing and inversion. The mixture was plated onto YPD agar (pH 4.5) and incubated at 30 °C for 8 h. After incubation, cells were washed twice with sterile distilled water and resuspended in SDCAA medium at an initial OD□□□ of 0.1, then grown overnight at 30 °C with shaking at 160 rpm. To evaluate mating efficiency, serial dilutions of the mated culture were plated on agar with either SDCAA or SDCAA supplemented with tryptophan. Mating efficiency was calculated as the ratio of colony counts on SDCAA to those on SDCAA with tryptophan.

4.6. Screening of the immune Fab library

To display the Fab fragments on the yeast surface, the Fab library was inoculated at a starting OD_{600} of 0.5 in 2× SGCAA medium and incubated at 20 °C with shaking at 160 rpm for 48 h. The expression of the surface-displayed Fabs was assessed by labeling the FLAG tag at the C-terminus of the LC with a mouse anti-FLAG antibody (Cat. MA1-91878, Invitrogen). The yeast was co-incubated with a biotinylated antigen for 1 hour at room temperature. After incubation, the cells were washed with PBSA (pH 7.2, containing 0.1% BSA). Secondary

labeling was performed using FITC-anti-mouse IgG (Cat. F0257, Sigma-Aldrich) and SA-PE (Cat. S866, Invitrogen) at 4 °C for 15 min. After a final wash with PBSA, the cells were analyzed and sorted by flow cytometry using an SH800S cell sorter (Sony Biotechnology Inc., San Jose, CA, USA). For negative selection, both MSLN-positive and MSLN-negative AsPC-1 cells were seeded in 6-well plates (6 x 10^5 cells/well) and incubated at 37 °C and 5% CO_2 for 2 d. Following incubation, the cells were fixed with 10% neutral-buffered formalin. To remove non-specific binders, 5 ×10^7 yeast cells (OD_{600} = 5) were added to wells containing MSLN-negative K562 cells and incubated at 4 °C with gentle shaking for 2 h. The supernatant was collected, and the wells were washed by adding 1 mL of ice-cold PBSA. For positive selection, the cells collected from the negative selection were incubated with MSLN-positive K562 cells. After incubation, the supernatant was discarded, and the cells were washed twice by adding 1 mL of iced-cold PBSA buffer per well. SDCAA medium was then added to each well and the cells were scrapped and cultured overnight at 30 °C with shaking at 160 rpm to promote cellular MSLN activity.

4.7. Preparation of recombinant anti-MSLN scFv proteins

Selected antibody genes were subcloned in-frame into the pMopac12 vector using Gibson Assembly (New England Biolabs, Ipswich, MA, USA). The resulting scFv-pMopac12 plasmid was transformed into *Escherichia coli* BL21 (DE3) cells, which were cultured in 500 mL of terrific broth supplemented with chloramphenicol at 37°C and 200 rpm until an OD_{600nm} of 0.6–0.8 was reached. Protein expression was induced with 0.5 mM IPTG, and the cultures were incubated for an additional 16 h at 25 °C with shaking at 160 rpm. Cells were harvested by centrifugation at 12 000 *g* for 1 hour and resuspended in 32 mL Tris-sucrose solution (pH 7.5; 100 mM Tris and 0.75 M sucrose). Lysozyme (20 mg/mL) was added to the suspension before incubation at 4°C with shaking. The cells were treated with 1 mM EDTA

(pH 8.0) and incubated once more. The periplasmic fraction was collected by centrifugation and filtration. His-tagged recombinant scFv proteins were purified using affinity chromatography.

4.8. ELISA of anti-MSLN scFvs

The binding activities of anti-MSLN scFvs were assessed by ELISA. Each well of 96-well MaxiSorp microplates was coated with 100 ng of scFvs and incubated overnight at 4 °C. After blocking with 3% PBSA for 1 hour at room temperature, biotinylated MSLN-His antigens were serially diluted and added to the wells. Plates were incubated at room temperature for 1 hour, washed with PBST, treated with streptavidin-HRP (1:40,000, Abcam, Cambridge, MA, USA), and incubated for 1 hour at room temperature. After washing, TMB substrate was added, the reaction was stopped with 2 M H_2SO_4, and absorbance at 450 nm was measured using the Infinite 200 PRO NanoQuant microplate reader (Tecan Trading AG).

4.9. Competitive ELISA of anti-MSLN scFvs

Each well of 96-well MaxiSorp microplates was coated with 100 ng scFv and incubated overnight at 4 °C. After blocking with 3% PBSA for 1 hour at room temperature, biotinylated MSLN-His antigens (200 nM) or preincubated biotinylated MSLN-His (100 nM) and anti-MSLN scFv (200 nM) complexes were added to the wells. Plates were incubated at room temperature for 1 hour, washed with PBST, treated with streptavidin-HRP (1:40,000, Abcam), and incubated for 1 h at room temperature. After washing, TMB substrate was added, the reaction was stopped with 2 M H_2SO_4, and absorbance at 450 nm was measured using the Infinite 200 PRO NanoQuant microplate reader (Tecan Trading AG). The outcomes were calculated by normalizing the antigen-only signal to 100% and expressing the measured signals as a percentage of this value.

4.10. Cell binding assay of anti-MSLN scFvs

$MSLN^+$ K562 and $MSLN^-$ K562 (5×10^4) cells were resuspended in PBSF, plated in a 96-well round-bottom plate, centrifuged at 300 *g* for 3 min, and the cell pellets were washed with fresh PBSF. Recombinant anti-MSLN scFvs were added at various concentrations and incubated at 4 °C for1 hour. After incubation, the cell pellets were washed with fresh PBSF and then incubated with anti-HIS-FITC (1:400, Abcam) at 4 °C for 15 min. The cells were washed with PBSF and analyzed by BD FACSCanto II flow cytometer (BD Biosciences, San Jose, CA, USA) to quantify scFv binding.

4.11. *In silico* structure analysis

The three-dimensional structures of the scFvs were determined using AlphaFold3 (Google DeepMind [72]. The model with the highest predicted Local Distance Difference Test and TM score was selected for further analysis. Structural comparisons were conducted using PyMOL, and protein–protein docking of MSLN to each scFv was performed using the antibody docking mode in Maestro 13.6 (Schrödinger Suite; Schrödinger, New York, NY, USA), while masking non-CDR regions. Among the generated poses, the one with the strongest binding affinity (under default parameters) was selected for subsequent structural evaluation.

4.12. Surface plasmon resonance (SPR)

Binding kinetics of CLMS10 IgG were assessed using a BIAcore T200 instrument. The mature form of MSLN was immobilized onto CM5 sensor chips via amine coupling, following the manufacturer's guidelines (Cytiva, Marlborough, MA, USA). HBS EP buffer (BR100669, Cytiva) was used as the running buffer. CLMS10 IgG, prepared in a serial

dilution, was injected at 30 μL/min for 120 s, followed by a 5-min dissociation phase. The chip was then regenerated by sequential 30-s injections of 5 mM NaOH and 0.5 M arginine (pH 8.0). Equilibrium dissociation constants (K_D) were derived by fitting the data to a 1:1 Langmuir model using BIAevaluation 3.2 software (Cytiva). Each K_D value represents the mean from three independent experiments (n = 3).

4.13. Immunohistochemistry (IHC)

We evaluated the binding capacity of CLMS10 IgG on human pancreatic cancer tissue using PDAC tumor tissue microarrays (PA482a Tissue Array, Derwood, MD, USA). Tissue sections were baked at 60 °C in a drying oven for 30 min, followed by deparaffinization and rehydration. Antigen retrieval was performed using Epitope Retrieval Solution (Bond Polymer Refine Detection kit, DS9800; Leica Biosystems, Nußloch, Germany). After blocking, the sections were incubated for 30 min with CLMS10 IgG (1.22 mg/mL, 1:30 dilution) and treated with 3,3′-diaminobenzidine (DAB) substrate (Bond Polymer Refine Detection kit, DS9800, Leica Biosystems) for signal detection. The slides were mounted and imaged using an Olympus BX53 microscope (Olympus Corporation, Tokyo, Japan). All IHC staining procedures were conducted following the standard protocols of the Pathology Specimen Production Center at Seoul National University.

4.14. Isolation and *ex vivo* expansion of human primary NK (pNK) cells.

PBMCs were purchased from Lonza (Walkersville, MD, USA). NK cells were cultured using medium from Miltenyi Biotec (Bergisch Gladbach, Germany). pNK cells were cultured and maintained in the presence of IL2 (200 IU/mL; PeproTech) and IL15 (10 ng/mL; PeproTech), along with K562 feeder cells obtained from American Type Culture Collection (Manassas, VA, USA). Following a 2-week expansion period, pNK cells were isolated using an NK cell

isolation kit (Miltenyi Biotec) according to the manufacturer's guidelines.

4.15. Vector construction and linRNA *in vitro* transcription (IVT) preparation

To construct the CAR plasmid, the novel scFv containing the second-generation CAR construct and GFP were cloned into the pmREX plasmid vector using the EZ-Fusion™ HT Cloning Kit (Cat. EZ015TL, Enzynomics, Daejeon, Republic of Korea) along with the SS1 (US Patent: US7081518) and 15B6 (US Patent: US7081518B1) scFv DNA fragments. The sequences of the novel scFvs were cloned into template DNA for mRNA synthesis. IVT of mRNA was performed using a linearized plasmid vector as the template and a MEGAscript™ T7 transcription kit (Cat. AMB13345, Invitrogen). The synthesized mRNA was capped with CleanCap® Reagent AG (Cat. N-7113, Trilink, San Diego, CA, USA). mRNA was precipitated using lithium chloride, purified, and the yield was measured using a NanoDrop 1000 UV Visible Spectrophotometer (ThermoFisher Scientific).

4.16. CAR-NK cells generated via electroporation of circRNA and IVT mRNA.

circRNA construct, designed as a second-generation CAR incorporating either the SS1 or CLMS10 scFv, was provided by GenScript (Nanjing, China). Expanded pNK cells were collected by centrifugation at 1500 rpm for 5 min and removing the culture medium. Cells were washed twice with 10mL DPBS and re-suspended in Resuspension Buffer T from a Neon™ Transfection System 100 μL Kit (4.0 × 10□ cells/mL; Invitrogen). CAR-NK cells were generated via IVT using 1 μg mRNA per 10□ cells. The mRNA was mixed thoroughly with 100 μL of cells suspended in Resuspension Buffer T buffer. Electroporation was performed using a Neon® Transfection System (Invitrogen) to facilitate intracellular mRNA delivery. For circCAR-NK generation, 0.5 μg of circRNA per 10□ cells was used for electroporation. In the case of multiple transfections, the concentration of each mRNA was

adjusted based on its corresponding molecular weight (bp size) to achieve the appropriate molarity, and the final concentration per 10^{6} cells was used for electroporation.

4.17. linCAR-T cell production

PBMCs were thawed and seeded in 24-well TC-treated plates (Cat. #CLS3524, Corning, NY, USA) that had been pre-coated for 3 h at 37 °C with 10 μg/mL anti-human CD3ε antibody (Cat. #16-0037-85, eBioscience, San Diego, CA, USA) in DPBS. Cells were cultured in AIM-V medium (Cat. #12055-091, Gibco) supplemented with IL-2 (200 IU/mL; PeproTech), GlutaMAX (100X; Cat. #35050061, Gibco), and 2 μg/mL anti-human CD28 antibody (Cat. #16-0289-85, eBioscience). After 24 h of incubation at 37°C in 5 % CO_2, additional AIM-V medium was added depending on the cell condition. T cell culture was conducted using medium RPMI1640 (Welgene) supplemented with IL2 (200 IU/mL). Primary T cells were expanded and harvested by centrifugation at 1800 rpm for 5 min and removing the culture medium. The cells were washed twice with 10 mL of DPBS and resuspended in Resuspension Buffer T (Invitrogen). The final cell concentration was adjusted to 4.0×10^{6} cells/mL. IVT of mRNA encoding the CAR construct was conducted at 1 μg per 10^{6} cells after thorough mixing in a 100 μL cell suspension. Electroporation was performed using the Neon® Transfection System (Invitrogen) under the following conditions: 1600 V, 10 ms, three pulses.

4.18. Flow cytometry

Collected cells were washed three times with staining buffer (DPBS supplemented with 2% FBS) and stained with eBioscience™ Fixable Viability Dye eFluor™ 780 (Thermo Fisher Scientific) for 20 min at 4°C. After staining, the cells were washed twice with staining buffer and then incubated with cell surface antibodies for 20 min at 4°C. Following incubation, the

cells were washed again and resuspended in 300 μL staining buffer prior to analysis. Flow cytometric analysis was performed using a CytoFLEX flow cytometer (Beckman Coulter Life Sciences, Munich, Germany), and data were analyzed using FlowJo software (BD Biosciences).

4.19. Live cell imaging-based Caspase-3/7 assay

To evaluate linCAR-NK cell candidates, Capan-2 cells were stained using a CellTrace™ Violet Cell Proliferation Kit (Invitrogen) according to the manufacturer's instructions. IVT of linCAR-NK cells involved GFP linked to the CAR construct via a P2A sequence. For the assay, Capan-2 cells were co-cultured with CAR-NK cells at a 2.5:1 effector:target (E:T) ratio in 100 μL co-culture medium supplemented with IL-2 (200 IU/mL). To measure the apoptosis in real-time, CellEvent™ Caspase-3/7 Detection Reagents RED (100x; Invitrogen) was added to the culture wells. The plates were placed into a BioTeck Lionheart FX live cell imaging system (Agilent Technologies, Santa Clara, CA, USA) and incubated for 12 h to monitor Caspase-3/7 activation as an indicator of apoptosis. Images were captured at the indicated times using the automated live-cell imager.

4.20. Luminescence-based cancer-killing assay

We assessed the cytotoxic effects of NK cells in NanoLuc luciferase (Luc)-overexpressing cancer cells [20, 73]. Capan-2-Luc or SK-O-V3-Luc cancer cells were co-cultured with pNK cells at the indicated E:T ratios. Following co-culture, cancer cell viability was determined in terms of luciferase activity measured using a Nano-Glo® luciferase assay system (Promega, Madison, WI, USA) according to the manufacturer`s instructions.

4.21. Shedding inhibition assay

To access the impact of solMSLN on CAR-NK cell activity, a luminescence-based cancer-killing assay was performed. Cancer cells were co-cultured with CAR-NK cells at the indicated E:T ratios for 12 h in IL2 (200 IU/mL)-supplemented medium with or without solMSLN at concentrations up to 100 µg/mL.

For the CD107a degranulation assay, matMSLN protein (20 µg/mL) coated 96-well plates were seeded with CAR-NK cells (1.0 × 10□ cells/well) and stimulated for 4 h with or without solMSLN (50 µg/mL). During stimulation, CD107a surface expression was assessed using APC-conjugated anti-CD107a antibody (1:100; Cat. 328620, BioLegend, San Diego, CA, USA) and BD GolgiStop containing Monensin (Cat. 554724, BD Bioscience). After 4 h, cells were stained with a viability dye and analyzed by flow cytometry using FlowJo software (BD Biosciences).

4.22. Cell avidity assay

Monolayer Capan-2 cells (5.0□×□10□/mL) were seeded into pre-coated z-Movi® chips (LUMICKS, Amsterdam, Netherlands) at 20□µL per well to achieve 60–80% confluency. linCAR-NK cells were harvested and labeled with Vybrant™ DiD Cell-Labeling Solution (5□µL/test; Cat. V22887, Invitrogen) following the manufacturer's protocol. After 15 minutes of staining, labeled linCAR-NK cells (1.0□×□10□/mL) were loaded into the chips (20□µL per test) and co-incubated with the adherent monolayer cells for 10 minutes. An acoustic force ramp (0–1000 pN over 2.5 min) was then applied using the z-Movi® Cell Avidity Analyzer (LUMICKS) to quantify the interaction strength between effector and target cells. Avidity was assessed via image acquisition using both brightfield and fluorescence channels and analyzed using Oceon™ software (LUMICKS). Monolayer integrity and the detachment of tracked cells were recorded and quantified as measures of cell–cell avidity.

4.23. Trogocytosis assay

To assess trogocytosis in CAR-NK cells, Capan-2 cells were seeded in a 48-well plate (1.0×10^5 cells/well) and incubated for 12 h; CAR-NK cells were added at a 1:1 ratio and co-cultured for 4 h. Cell–cell interactions were stimulated via brief centrifugation (200 *g*, 30 s, 4 °C). Following co-culture, cells were harvested in cold DPBS and stained with anti-Mesothelin antibody (Cat. ab196235; 1:1,000; Abcam) and CD56-APC (Cat.17-0566-42; 1:100; Invitrogen) to identify NK cells that had undergone trogocytosis. The degree of trogocytosis was determined as the percentage of $MSLN^+$ cells within the $CD56^+$ NK cell population using CytoFLEX (Beckman Coulter Life Sciences).

4.24. Metabolic Activity Assay

To promote cell adherence, Seahorse XFe96/XF Pro Cell Culture Microplate (Agilent Technologies) were pre-coated with poly-D-lysine (Cat. A-003-E, Sigma-Aldrich, Sigma-Aldrich, St. Louis, MO, USA). linCAR-NK cells were seeded at 2.5×10^5 cells per well in Seahorse XF DMEM (pH 7.4; Cat. 103575-100, Agilent Technologies) supplemented with 10 mM glucose, 1 mM pyruvate, and 2 mM glutamine. Oxygen consumption rate (OCR) was measured using a Seahorse XF Pro analyzer (Agilent Technologies). To assess mitochondrial function and metabolic activity, oligomycin (1.5 μM), FCCP (1 μM), rotenone (0.5 μM), and antimycin A (0.5 μM) were sequentially added at defined time points.

4.25. Detection of secreted solMSLN in co-culture media

Capan-2 cancer cells and CAFs were seeded in 100 mm plates, either separately or together (2×10□ cells). After 24 h in serum-containing media, cells were washed and incubated with serum-free RPMI1640 supplemented with 1% AA and 10 ng/mL FGF for 48 h. Conditioned media were collected and concentrated 40-fold using Amicon® Ultra centrifugal filters (10

kDa MWCO; Merck Millipore, Darmstadt, Germany) at 4000 rpm at 4°C for 45 min. The concentrated media were used for western blot analysis.

4.26. Western blot analysis

Cells were lysed using RIPA buffer (Thermo Fisher Scientific,) containing a protease and/or phosphatase inhibitor cocktail. Proteins from lysates or conditioned media were separated by SDS-PAGE and transferred onto polyvinylidene difluoride membranes blocked with 5% skim milk in 0.2% Tween 20/TBS for 2 h at room temperature and incubated overnight at 4°C with anti-mesothelin antibody (1:1000; Cat. ab196235, Abcam). After washing, membranes were incubated with HRP-conjugated goat anti-rabbit IgG (1:10,000; Cat. 32460, Invitrogen) and visualized using SuperSignal West Pico PLUS substrate (Cat. 34580, Thermo Fisher Scientific) with a ChemiDoc imaging system (Bio-Rad Laboratories, Hercules, CA, USA).

4.27. IFN-γ detection

To evaluate cytokine secretion in vitro, various NK cell subsets were co-cultured with Capan-2 cells. After 48 h of incubation, culture supernatants were harvested and IFNγ levels were quantified using a human IFNγ ELISA kit (Cat. DIF50C, R&D Systems, Minneapolis, MN, USA) according to the manufacturer's instructions.

4.28. Lentivirus production and titration

HEK293T cells were co-transfected with a CAR-expressing plasmid, the psPAX2 packaging plasmid, and a Baboon envelope plasmid in a 3:2:1 ratio using polyethylenimine (PEI) transfection reagent (Polysciences Inc., USA). After 24 and 48 hours, the supernatant containing the lentivirus was collected and concentrated using the Lenti-X Concentrator (Takara, Kusatsu, Shiga Japan). The viral titer was then determined using the Lenti-X p24

Rapid Titer Kit (Takara) following the manufacturer's protocol [73].

4.29. linRNA and circCAR-NK-mediated serial killing assay

To assess serial killing capacity, linCAR and circCAR-NK cells were co-cultured with Capan-2-Luc cells (4 x 10^4 Capan-2-Luc cells/well) at a 1:1 ET ratio. After 12 h of co-culture, CAR-NK cells were collected by centrifugation, resuspended in fresh IL2-supplemented media (200 IU/mL), and transferred onto newly seeded Capan-2 -Luc cells. This process was repeated multiple times to evaluate the duration of cytotoxicity. Cytotoxicity at each round was quantified using a luminescence-based assay. For solMSLN shedding inhibition, the assay was conducted in media containing 50 µg/mL recombinant solMSLN protein.

4.30. *In vivo* efficacy of CAR-NK cells

All animal procedures were conducted in accordance with institutional guidelines and approved by the Institutional Animal Care and Use Committees of KIST (KIST–2024–079). A metastatic tumor model reflecting TME with high solMSLN secretion was established via intraperitoneal injection of either 3 × 10□ AsPC-1-MSLN-Luc cells alone or a mixture of AsPC-1-MSLN-Luc and CAF6 cells at a 3:1 ratio. After 11 d, mice were randomly divided into seven groups and treated under various conditions. Tumor-bearing mice each received three intravenous administrations of 1 × 10□ linCAR-NK, circCAR-NK, or $_{LV}$CAR-NK cells. Tumor progression was monitored via in vivo luciferase imaging using an IVIS Spectrum imaging system (Revvity, Waltham, MA, USA) following intravenous injection of a luciferin substrate solution (Promega) under isoflurane anesthesia. Tumor burden was quantified by measuring the average radiance (photons/s/cm²/sr).

Declaration of competing interest

C-H.L. and J.S.H. (KR10-2024-0059322) and M.J., C.-H.L., J.Y.J., and J.S.H. are listed as inventors on provisional patents (KR10-2025-0013774). The authors declare no other competing interests.

Acknowledgments

This work was supported by the National Research Foundation (NRF) of Korea, funded by the Korean Government (grant nos. RS-2023-NR076986, RS-2024-00509114, RS-2025-02216943, and RS-2023-00278980). Additional support was provided by the KIST Institutional Program (grant no. 2E33761) and Seoul National University Hospital (SNUH) Research Fund (grant no. 03-2024-3030).

CRediT authorship contribution statement

Joo-Yoon Chung: Writing – review & editing, Methodology, Investigation, Formal analysis, Data curation. **Jisu Hong:** Writing – review & editing, Methodology, Formal analysis, Data curation. **Su-Min Yee:** Methodology, Formal analysis, Data curation. **Hye Won Lim:** Formal analysis, Data curation. **Dahye Lee:** Methodology, Formal analysis, Data curation. **Sangwon Yoon:** Methodology. **Seung-Hwan Lee:** Methodology. **Yujin Jung:** Data curation. **Seung hun Shin:** Methodology. **Song Cheol Kim:** Resources. **Chang-Han Lee:** Writing – review & editing, Writing – original draft, Methodology, Supervision, Funding acquisition, Conceptualization. **Mihue Jang:** Writing – review & editing, Writing – original draft, Methodology, Supervision, Funding acquisition, Conceptualization.

Data availability statement

All data that support the findings of this study are available from the corresponding author upon reasonable request.

References

[1] E. Vivier, D.H. Raulet, A. Moretta, M.A. Caligiuri, L. Zitvogel, L.L. Lanier, W.M. Yokoyama, S. Ugolini, Innate or adaptive immunity? The example of natural killer cells, Science 331(6013) (2011) 44-9.

[2] T.J. Laskowski, A. Biederstadt, K. Rezvani, Natural killer cells in antitumour adoptive cell immunotherapy, Nat Rev Cancer 22(10) (2022) 557-575.

[3] Y. Li, D.L. Hermanson, B.S. Moriarity, D.S. Kaufman, Human iPSC-Derived Natural Killer Cells Engineered with Chimeric Antigen Receptors Enhance Anti-tumor Activity, Cell Stem Cell 23(2) (2018) 181-192 e5.

[4] D. Marin, Y. Li, R. Basar, H. Rafei, M. Daher, J. Dou, V. Mohanty, M. Dede, Y. Nieto, N. Uprety, S. Acharya, E. Liu, J. Wilson, P. Banerjee, H.A. Macapinlac, C. Ganesh, P.F. Thall, R. Bassett, M. Ammari, S. Rao, K. Cao, M. Shanley, M. Kaplan, C. Hosing, P. Kebriaei, L.J. Nastoupil, C.R. Flowers, S.M. Moseley, P. Lin, S. Ang, U.R. Popat, M.H. Qazilbash, R.E. Champlin, K. Chen, E.J. Shpall, K. Rezvani, Safety, efficacy and determinants of response of allogeneic CD19-specific CAR-NK cells in CD19(+) B cell tumors: a phase 1/2 trial, Nat Med 30(3) (2024) 772-784.

[5] A. Ghobadi, V. Bachanova, K. Patel, J.H. Park, I. Flinn, P.A. Riedell, C. Bachier, C.S. Diefenbach, C. Wong, C. Bickers, L. Wong, D. Patel, J. Goodridge, M. Denholt, B. Valamehr, R.L. Elstrom, P. Strati, Induced pluripotent stem-cell-derived CD19-directed chimeric antigen

receptor natural killer cells in B-cell lymphoma: a phase 1, first-in-human trial, Lancet 405(10473) (2025) 127-136.

[6] M.J. Lee, F. Cichocki, J.S. Miller, CAR therapies: development, design, and implementation, J Allergy Clin Immunol (2025).

[7] A. Page, N. Chuvin, J. Valladeau-Guilemond, S. Depil, Development of NK cell-based cancer immunotherapies through receptor engineering, Cell Mol Immunol 21(4) (2024) 315-331.

[8] M. Daher, K. Rezvani, Next generation natural killer cells for cancer immunotherapy: the promise of genetic engineering, Curr Opin Immunol 51 (2018) 146-153.

[9] N. Lamers-Kok, D. Panella, A.M. Georgoudaki, H. Liu, D. Ozkazanc, L. Kucerova, A.D. Duru, J. Spanholtz, M. Raimo, Natural killer cells in clinical development as non-engineered, engineered, and combination therapies, J Hematol Oncol 15(1) (2022) 164.

[10] P. Chockley, S.L. Patil, S. Gottschalk, Transient blockade of TBK1/IKKepsilon allows efficient transduction of primary human natural killer cells with vesicular stomatitis virus G-pseudotyped lentiviral vectors, Cytotherapy 23(9) (2021) 787-792.

[11] H.E. Gouvarchin Ghaleh, M. Bolandian, R. Dorostkar, A. Jafari, M.F. Pour, Concise review on optimized methods in production and transduction of lentiviral vectors in order to facilitate immunotherapy and gene therapy, Biomed Pharmacother 128 (2020) 110276.

[12] A. Girard-Gagnepain, F. Amirache, C. Costa, C. Levy, C. Frecha, F. Fusil, D. Negre, D. Lavillette, F.L. Cosset, E. Verhoeyen, Baboon envelope pseudotyped LVs outperform VSV-G-LVs for gene transfer into early-cytokine-stimulated and resting HSCs, Blood 124(8) (2014) 1221-31.

[13] A.B.L. Colamartino, W. Lemieux, P. Bifsha, S. Nicoletti, N. Chakravarti, J. Sanz, H. Romero, S. Selleri, K. Beland, M. Guiot, C. Tremblay-Laganiere, R. Dicaire, L. Barreiro, D.A. Lee, E. Verhoeyen, E. Haddad, Efficient and Robust NK-Cell Transduction With

Baboon Envelope Pseudotyped Lentivector, Front Immunol 10 (2019) 2873.

[14] K. Noguchi, Y. Ikawa, M. Takenaka, Y. Sakai, T. Fujiki, R. Kuroda, M. Chappell, V. Ghiaccio, S. Rivella, T. Wada, Protocol for a high titer of BaEV-Rless pseudotyped lentiviral vector: Focus on syncytium formation and detachment, J Virol Methods 314 (2023) 114689.

[15] R. Hassan, A. Thomas, C. Alewine, D.T. Le, E.M. Jaffee, I. Pastan, Mesothelin Immunotherapy for Cancer: Ready for Prime Time?, J Clin Oncol 34(34) (2016) 4171-4179.

[16] J.R. Faust, D. Hamill, E.A. Kolb, A. Gopalakrishnapillai, S.P. Barwe, Mesothelin: An Immunotherapeutic Target beyond Solid Tumors, Cancers (Basel) 14(6) (2022).

[17] A. Morello, M. Sadelain, P.S. Adusumilli, Mesothelin-Targeted CARs: Driving T Cells to Solid Tumors, Cancer Discov 6(2) (2016) 133-46.

[18] S.S. Kachala, A.J. Bograd, J. Villena-Vargas, K. Suzuki, E.L. Servais, K. Kadota, J. Chou, C.S. Sima, E. Vertes, V.W. Rusch, W.D. Travis, M. Sadelain, P.S. Adusumilli, Mesothelin overexpression is a marker of tumor aggressiveness and is associated with reduced recurrence-free and overall survival in early-stage lung adenocarcinoma, Clin Cancer Res 20(4) (2014) 1020-8.

[19] M. Malla, S.K. Deshmukh, S. Wu, T. Samec, D.C. Olevian, R. El Naili, B. El-Rayes, J. Xiu, A. Farrell, H.J. Lenz, E. Lou, S. Goel, D. Spetzler, R.M. Goldberg, L. Hazlehurst, Mesothelin expression correlates with elevated inhibitory immune activity in patients with colorectal cancer, Cancer Gene Ther 31(10) (2024) 1547-1558.

[20] Y.E. Lee, G.Y. Go, E.Y. Koh, H.N. Yoon, M. Seo, S.M. Hong, J.H. Jeong, J.C. Kim, D. Cho, T.S. Kim, S.C. Kim, E. Jun, M. Jang, Synergistic therapeutic combination with a CAF inhibitor enhances CAR-NK-mediated cytotoxicity via reduction of CAF-released IL-6, J Immunother Cancer 11(2) (2023).

[21] Q. Le, S. Castro, T. Tang, A.M. Loeb, T. Hylkema, C.N. McKay, L. Perkins, S. Srivastava, L. Call, J. Smith, A. Leonti, R. Ries, L. Pardo, M.R. Loken, C. Correnti, S.

Fiorenza, C.J. Turtle, S. Riddell, K. Tarlock, S. Meshinchi, Therapeutic Targeting of Mesothelin with Chimeric Antigen Receptor T Cells in Acute Myeloid Leukemia, Clin Cancer Res 27(20) (2021) 5718-5730.

[22] P. Awuah, T.K. Bera, M. Folivi, O. Chertov, I. Pastan, Reduced Shedding of Surface Mesothelin Improves Efficacy of Mesothelin-Targeting Recombinant Immunotoxins, Mol Cancer Ther 15(7) (2016) 1648-55.

[23] X. Liu, M. Onda, N. Watson, R. Hassan, M. Ho, T.K. Bera, J. Wei, A. Chakraborty, R. Beers, Q. Zhou, A. Shajahan, P. Azadi, J. Zhan, D. Xia, I. Pastan, Highly active CAR T cells that bind to a juxtamembrane region of mesothelin and are not blocked by shed mesothelin, Proc Natl Acad Sci U S A 119(19) (2022) e2202439119.

[24] Q. Xiao, X. Zhang, L. Tu, J. Cao, C.S. Hinrichs, X. Su, Size-dependent activation of CAR-T cells, Sci Immunol 7(74) (2022) eabl3995.

[25] S. Srivastava, S.R. Riddell, Engineering CAR-T cells: Design concepts, Trends Immunol 36(8) (2015) 494-502.

[26] R.C. Sterner, R.M. Sterner, CAR-T cell therapy: current limitations and potential strategies, Blood Cancer J 11(4) (2021) 69.

[27] P. Celichowski, M. Turi, S. Charvatova, D. Radhakrishnan, N. Feizi, Z. Chyra, M. Simicek, T. Jelinek, J.R. Bago, R. Hajek, M. Hrdinka, Tuning CARs: recent advances in modulating chimeric antigen receptor (CAR) T cell activity for improved safety, efficacy, and flexibility, J Transl Med 21(1) (2023) 197.

[28] D. Liu, S. Badeti, G. Dotti, J.G. Jiang, H. Wang, J. Dermody, P. Soteropoulos, D. Streck, R.B. Birge, C. Liu, The Role of Immunological Synapse in Predicting the Efficacy of Chimeric Antigen Receptor (CAR) Immunotherapy, Cell Commun Signal 18(1) (2020) 134.

[29] M. Mazinani, F. Rahbarizadeh, CAR-T cell potency: from structural elements to vector backbone components, Biomark Res 10(1) (2022) 70.

[30] D.S. Baek, S.W. Park, C. Adams, D.S. Dimitrov, Y.S. Kim, Yeast Mating as a Tool for Highly Effective Discovery and Engineering of Antibodies via Display Methodologies, Methods Mol Biol 2491 (2022) 313-333.

[31] D.S. Baek, Y.S. Kim, Construction of a large synthetic human Fab antibody library on yeast cell surface by optimized yeast mating, J Microbiol Biotechnol 24(3) (2014) 408-20.

[32] J. Zhang, S. Qiu, Y. Zhang, M. Merino, P. Fetsch, I. Avital, A. Filie, I. Pastan, R. Hassan, Loss of mesothelin expression by mesothelioma cells grown in vitro determines sensitivity to anti-mesothelin immunotoxin SS1P, Anticancer Res 32(12) (2012) 5151-8.

[33] Y. Zhang, L. Xiang, R. Hassan, I. Pastan, Immunotoxin and Taxol synergy results from a decrease in shed mesothelin levels in the extracellular space of tumors, Proc Natl Acad Sci U S A 104(43) (2007) 17099-104.

[34] C.H. Lee, G. Romain, W. Yan, M. Watanabe, W. Charab, B. Todorova, J. Lee, K. Triplett, M. Donkor, O.I. Lungu, A. Lux, N. Marshall, M.A. Lindorfer, O.R. Goff, B. Balbino, T.H. Kang, H. Tanno, G. Delidakis, C. Alford, R.P. Taylor, F. Nimmerjahn, N. Varadarajan, P. Bruhns, Y.J. Zhang, G. Georgiou, IgG Fc domains that bind C1q but not effector Fcgamma receptors delineate the importance of complement-mediated effector functions, Nat Immunol 18(8) (2017) 889-898.

[35] M. Kim, X. Bai, H. Im, J. Yang, Y. Kim, M.M. Kim, Y. Oh, Y. Jeon, H. Kwon, S. Lee, C.H. Lee, Construction and validation of a synthetic phage-displayed nanobody library, Korean J Physiol Pharmacol 28(5) (2024) 457-467.

[36] S. Tomar, J. Zhang, M. Khanal, J. Hong, A. Venugopalan, Q. Jiang, M. Sengupta, M. Miettinen, N. Li, I. Pastan, M. Ho, R. Hassan, Development of Highly Effective Anti-Mesothelin hYP218 Chimeric Antigen Receptor T Cells With Increased Tumor Infiltration and Persistence for Treating Solid Tumors, Mol Cancer Ther 21(7) (2022) 1195-1206.

[37] M. Hamieh, A. Dobrin, A. Cabriolu, S.J.C. van der Stegen, T. Giavridis, J. Mansilla-Soto,

J. Eyquem, Z. Zhao, B.M. Whitlock, M.M. Miele, Z. Li, K.M. Cunanan, M. Huse, R.C. Hendrickson, X. Wang, I. Riviere, M. Sadelain, CAR T cell trogocytosis and cooperative killing regulate tumour antigen escape, Nature 568(7750) (2019) 112-116.

[38] Y. Li, R. Basar, G. Wang, E. Liu, J.S. Moyes, L. Li, L.N. Kerbauy, N. Uprety, M. Fathi, A. Rezvan, P.P. Banerjee, L. Muniz-Feliciano, T.J. Laskowski, E. Ensley, M. Daher, M. Shanley, M. Mendt, S. Acharya, B. Liu, A. Biederstadt, H. Rafei, X. Guo, L. Melo Garcia, P. Lin, S. Ang, D. Marin, K. Chen, L. Bover, R.E. Champlin, N. Varadarajan, E.J. Shpall, K. Rezvani, KIR-based inhibitory CARs overcome CAR-NK cell trogocytosis-mediated fratricide and tumor escape, Nat Med 28(10) (2022) 2133-2144.

[39] Y. Wang, A. Buck, B. Piel, L. Zerefa, N. Murugan, C.D. Coherd, A.G. Miklosi, H. Johal, R.N. Bastos, K. Huang, M. Ficial, Y.N. Laimon, S. Signoretti, Z. Zhong, S.M. Hoang, G.M. Kastrunes, M. Grimaud, A. Fayed, H.C. Yuan, Q.D. Nguyen, T. Thai, E.V. Ivanova, C.P. Paweletz, M.R. Wu, T.K. Choueiri, J.O. Wee, G.J. Freeman, D.A. Barbie, W.A. Marasco, Affinity fine-tuning anti-CAIX CAR-T cells mitigate on-target off-tumor side effects, Mol Cancer 23(1) (2024) 56.

[40] K. Shah, A. Al-Haidari, J. Sun, J.U. Kazi, T cell receptor (TCR) signaling in health and disease, Signal Transduct Target Ther 6(1) (2021) 412.

[41] Y. Peng, W. Zhang, Y. Chen, L. Zhang, H. Shen, Z. Wang, S. Tian, X. Yang, D. Cui, Y. He, X. Chang, Z. Feng, Q. Tang, Y. Mao, Engineering c-Met-CAR NK-92 cells as a promising therapeutic candidate for lung adenocarcinoma, Pharmacol Res 188 (2023) 106656.

[42] A.C. Issekutz, B. Derfalvi, F. Kasermann, D. Rowter, Potentiation of cytokine-induced proliferation of human Natural Killer cells by intravenous immunoglobulin G, Clin Immunol 161(2) (2015) 373-83.

[43] M. Shanley, M. Daher, J. Dou, S. Li, R. Basar, H. Rafei, M. Dede, J. Gumin, J. Pantaleomicronn Garciotaa, A.K. Nunez Cortes, S. He, C.M. Jones, S. Acharya, N.W.

Fowlkes, D. Xiong, S. Singh, H. Shaim, S.C. Hicks, B. Liu, A. Jain, M.F. Zaman, Q. Miao, Y. Li, N. Uprety, E. Liu, L. Muniz-Feliciano, G.M. Deyter, V. Mohanty, P. Zhang, S.E. Evans, E.J. Shpall, F.F. Lang, K. Chen, K. Rezvani, Interleukin-21 engineering enhances NK cell activity against glioblastoma via CEBPD, Cancer Cell 42(8) (2024) 1450-1466 e11.

[44] J.C. Sun, L.L. Lanier, NK cell development, homeostasis and function: parallels with CD8(+) T cells, Nat Rev Immunol 11(10) (2011) 645-57.

[45] E. Lasda, R. Parker, Circular RNAs: diversity of form and function, RNA 20(12) (2014) 1829-42.

[46] R.A. Wesselhoeft, P.S. Kowalski, F.C. Parker-Hale, Y. Huang, N. Bisaria, D.G. Anderson, RNA Circularization Diminishes Immunogenicity and Can Extend Translation Duration In Vivo, Mol Cell 74(3) (2019) 508-520 e4.

[47] R. Chen, S.K. Wang, J.A. Belk, L. Amaya, Z. Li, A. Cardenas, B.T. Abe, C.K. Chen, P.A. Wender, H.Y. Chang, Engineering circular RNA for enhanced protein production, Nat Biotechnol 41(2) (2023) 262-272.

[48] E. Karamitopoulou, Tumour microenvironment of pancreatic cancer: immune landscape is dictated by molecular and histopathological features, Br J Cancer 121(1) (2019) 5-14.

[49] S. Regis, A. Dondero, F. Caliendo, C. Bottino, R. Castriconi, NK Cell Function Regulation by TGF-beta-Induced Epigenetic Mechanisms, Front Immunol 11 (2020) 311.

[50] H. Shaim, M. Shanley, R. Basar, M. Daher, J. Gumin, D.B. Zamler, N. Uprety, F. Wang, Y. Huang, K. Gabrusiewicz, Q. Miao, J. Dou, A. Alsuliman, L.N. Kerbauy, S. Acharya, V. Mohanty, M. Mendt, S. Li, J. Lu, J. Wei, N.W. Fowlkes, E. Gokdemir, E.L. Ensley, M. Kaplan, C. Kassab, L. Li, G. Ozcan, P.P. Banerjee, Y. Shen, A.L. Gilbert, C.M. Jones, M. Bdiwi, A.K. Nunez-Cortes, E. Liu, J. Yu, N. Imahashi, L. Muniz-Feliciano, Y. Li, J. Hu, G. Draetta, D. Marin, D. Yu, S. Mielke, M. Eyrich, R.E. Champlin, K. Chen, F.F. Lang, E.J. Shpall, A.B. Heimberger, K. Rezvani, Targeting the alphav integrin/TGF-beta axis improves

natural killer cell function against glioblastoma stem cells, J Clin Invest 131(14) (2021).

[51] H. Huang, Z. Wang, Y. Zhang, R.N. Pradhan, D. Ganguly, R. Chandra, G. Murimwa, S. Wright, X. Gu, R. Maddipati, S. Muller, S.J. Turley, R.A. Brekken, Mesothelial cell-derived antigen-presenting cancer-associated fibroblasts induce expansion of regulatory T cells in pancreatic cancer, Cancer Cell 40(6) (2022) 656-673 e7.

[52] J. Wu, W. Wu, B. Zhou, B. Li, Chimeric antigen receptor therapy meets mRNA technology, Trends Biotechnol 42(2) (2024) 228-240.

[53] X.F. Liu, M. Onda, J. Schlomer, L. Bassel, S. Kozlov, C.H. Tai, Q. Zhou, W. Liu, H.E. Tsao, R. Hassan, M. Ho, I. Pastan, Tumor resistance to anti-mesothelin CAR-T cells caused by binding to shed mesothelin is overcome by targeting a juxtamembrane epitope, Proc Natl Acad Sci U S A 121(4) (2024) e2317283121.

[54] X. Zhai, L. Mao, M. Wu, J. Liu, S. Yu, Challenges of Anti-Mesothelin CAR-T-Cell Therapy, Cancers (Basel) 15(5) (2023).

[55] R. Bari, M. Granzin, K.S. Tsang, A. Roy, W. Krueger, R. Orentas, D. Schneider, R. Pfeifer, N. Moeker, E. Verhoeyen, B. Dropulic, W. Leung, A Distinct Subset of Highly Proliferative and Lentiviral Vector (LV)-Transducible NK Cells Define a Readily Engineered Subset for Adoptive Cellular Therapy, Front Immunol 10 (2019) 2001.

[56] A.E. Metzloff, M.S. Padilla, N. Gong, M.M. Billingsley, X. Han, M. Merolle, D. Mai, C.G. Figueroa-Espada, A.S. Thatte, R.M. Haley, A.J. Mukalel, A.G. Hamilton, M.G. Alameh, D. Weissman, N.C. Sheppard, C.H. June, M.J. Mitchell, Antigen Presenting Cell Mimetic Lipid Nanoparticles for Rapid mRNA CAR T Cell Cancer Immunotherapy, Adv Mater 36(26) (2024) e2313226.

[57] Y. Zhang, C. Zhang, M. He, W. Xing, R. Hou, H. Zhang, Co-expression of IL-21-Enhanced NKG2D CAR-NK cell therapy for lung cancer, BMC Cancer 24(1) (2024) 119.

[58] P. Wong, J.A. Foltz, L. Chang, C.C. Neal, T. Yao, C.C. Cubitt, J. Tran, S. Kersting-

Schadek, S. Palakurty, N. Jaeger, D.A. Russler-Germain, N.D. Marin, M. Gang, J.A. Wagner, A.Y. Zhou, M.T. Jacobs, M. Foster, T. Schappe, L. Marsala, E. McClain, P. Pence, M. Becker-Hapak, B. Fisk, A.A. Petti, O.L. Griffith, M. Griffith, M.M. Berrien-Elliott, T.A. Fehniger, T-BET and EOMES sustain mature human NK cell identity and antitumor function, J Clin Invest 133(13) (2023).

[59] H.J. Hwang, Y.K. Kim, Molecular mechanisms of circular RNA translation, Exp Mol Med 56(6) (2024) 1272-1280.

[60] X. Liu, Y. Zhang, S. Zhou, L. Dain, L. Mei, G. Zhu, Circular RNA: An emerging frontier in RNA therapeutic targets, RNA therapeutics, and mRNA vaccines, J Control Release 348 (2022) 84-94.

[61] J. Moscarelli, D. Zahavi, R. Maynard, L.M. Weiner, The Next Generation of Cellular Immunotherapy: Chimeric Antigen Receptor-Natural Killer Cells, Transplant Cell Ther 28(10) (2022) 650-656.

[62] L. Peng, G. Sferruzza, L. Yang, L. Zhou, S. Chen, CAR-T and CAR-NK as cellular cancer immunotherapy for solid tumors, Cell Mol Immunol 21(10) (2024) 1089-1108.

[63] N.D. Huntington, J. Cursons, J. Rautela, The cancer-natural killer cell immunity cycle, Nat Rev Cancer 20(8) (2020) 437-454.

[64] Y.R. Li, Y. Fang, S. Niu, Y. Chen, Z. Lyu, L. Yang, Managing allorejection in off-the-shelf CAR-engineered cell therapies, Mol Ther (2024).

[65] E.M. McErlean, H.O. McCarthy, Non-viral approaches in CAR-NK cell engineering: connecting natural killer cell biology and gene delivery, J Nanobiotechnology 22(1) (2024) 552.

[66] S.W. Choi, J.W. Nam, Optimal design of synthetic circular RNAs, Exp Mol Med 56(6) (2024) 1281-1292.

[67] Y. Du, P.K. Zuber, H. Xiao, X. Li, Y. Gordiyenko, V. Ramakrishnan, Efficient circular

RNA synthesis for potent rolling circle translation, Nat Biomed Eng (2024).

[68] M. Tong, N. Palmer, A. Dailamy, A. Kumar, H. Khaliq, S. Han, E. Finburgh, M. Wing, C. Hong, Y. Xiang, K. Miyasaki, A. Portell, J. Rainaldi, A. Suhardjo, S. Nourreddine, W.L. Chew, E.J. Kwon, P. Mali, Robust genome and cell engineering via in vitro and in situ circularized RNAs, Nat Biomed Eng 9(1) (2025) 109-126.

[69] D.S. Lefler, S.A. Manobianco, B. Bashir, Immunotherapy resistance in solid tumors: mechanisms and potential solutions, Cancer Biol Ther 25(1) (2024) 2315655.

[70] M. Zhang, Y.Y. Zhang, Y. Chen, J. Wang, Q. Wang, H. Lu, TGF-beta Signaling and Resistance to Cancer Therapy, Front Cell Dev Biol 9 (2021) 786728.

[71] Y. Pan, H. Zhou, Z. Sun, Y. Zhu, Z. Zhang, J. Han, Y. Liu, Q. Wang, Regulatory T cells in solid tumor immunotherapy: effect, mechanism and clinical application, Cell Death Dis 16(1) (2025) 277.

[72] J. Abramson, J. Adler, J. Dunger, R. Evans, T. Green, A. Pritzel, O. Ronneberger, L. Willmore, A.J. Ballard, J. Bambrick, S.W. Bodenstein, D.A. Evans, C.C. Hung, M. O'Neill, D. Reiman, K. Tunyasuvunakool, Z. Wu, A. Zemgulyte, E. Arvaniti, C. Beattie, O. Bertolli, A. Bridgland, A. Cherepanov, M. Congreve, A.I. Cowen-Rivers, A. Cowie, M. Figurnov, F.B. Fuchs, H. Gladman, R. Jain, Y.A. Khan, C.M.R. Low, K. Perlin, A. Potapenko, P. Savy, S. Singh, A. Stecula, A. Thillaisundaram, C. Tong, S. Yakneen, E.D. Zhong, M. Zielinski, A. Zidek, V. Bapst, P. Kohli, M. Jaderberg, D. Hassabis, J.M. Jumper, Accurate structure prediction of biomolecular interactions with AlphaFold 3, Nature 630(8016) (2024) 493-500.

[73] S.H. Shin, Y.E. Lee, H.N. Yoon, C.M. Yuk, J.Y. An, M. Seo, S. Yoon, M.S. Oh, S.C. Shin, J.H. Kim, Y.J. Kim, J.C. Kim, S.C. Kim, M. Jang, An innovative strategy harnessing self-activating CAR-NK cells to mitigate TGF-beta1-driven immune suppression, Biomaterials 314 (2025) 122888.

1043

Figure Legends

Fig. 1. Streamlined chimeric antigen receptor (CAR) screening and circRNA-based CAR (circCAR)-natural killer (NK) cell development to overcome antigen shedding

Schematic workflow illustrating (1) antibody discovery using a yeast surface-display platform to isolate high-affinity clones targeting membrane-bound mesothelin (MSLN); (2) rapid CAR optimization via mRNA-engineering of NK cells for functional screening; and (3) development of persistent shed resistant CAR-NK cells using circRNA.

Fig. 2. Screening and characterization of mature mesothelin (matMSLN)-specific scFvs

(A) Schematic representation of matMSLN (residues 296–606) and its soluble counterpart (solMSLN, residues 296–592). The top bar depicts full-length matMSLN ending in a GPI anchor at residue 606; the bottom bar represents solMSLN, which lacks a C-terminal GPI-anchoring region. The corresponding amino acid sequence is aligned with annotate residue positions. **(B)** Heatmap showing levels and antigen-binding affinities of individual scFv clones. Yeast-displayed clones were analyzed by flow cytometry using an anti-FLAG antibody (expression) and 10 nM biotinylated matMSLN or solMSLN (binding). Clones are ranked by mean fluorescence intensity (MFI). **(C-D)** ELISA-based binding of recombinant anti-MSLN scFvs to matMSLN (C) and solMSLN (D). Binding in immobilized scFvs incubated with serial dilutions of biotinylated antigen and detected using streptavidin-HRP. **(E-F)** Flow cytometry of cell surface binding by scFvs to $MSLN^+$ (E) and $MSLN^-$ K562 cells (F). Serially diluted antibodies were incubated with cells, and bound scFvs were detected using an anti-His-FITC secondary antibody. **(G)** Epitope binning of anti-MSLN scFvs (CLMS10, CLMS32, CLMS36, CLMS76, CLMS95, SS1, and 15B6) by competitive ELISA. Immobilized scFvs were challenged with biotinylated matMSLN pre-incubated with competing antibodies. Heatmap intensity reflects degree of competitive binding, indicating

epitope overlap. **(H)** Predicted epitope mapping of anti-MSLN scFvs based on binning data. According to UniProt annotations, the extracellular domain of MSLN is divided into Region I (residues 296–398), Region II (399–494), and Region III (495–606). Three independent experiments were performed; data are presented as mean ± standard deviation (s.d.).

Fig. 3. mRNA-based screening identifies CLMS10 as a potent shedding-resistant CAR construct in NK cells.

(A) Generation of linear mRNA-based CAR (linCAR)-NK cells via electroporation (EP) of human primary NK cells. **(B-C)** Establishment of high-throughput screening platform for evaluating CAR-NK cytotoxicity against Capan-2 cells. **(B)** Visualization of CAR-NK-mediated cancer cell killing. Capan-2 cells were stained with CellTrace™ Violet Cell (blue) and live-cell Caspase-3/7 dye (red), and co-cultured with CAR-NK cells (green). **(C)** Quantification of apoptotic cancer cells based on Caspase-3/7 activation (n = 3). **(D)** Shedding inhibition assay for determining CAR-NK cytotoxicity in the presence of increasing concentrations of solMSLN (residues 296–592); dashed lines indicate baseline cytotoxicity of allogeneic NK cells. **(E)** CD107a activation in CAR-NK cells stimulated with matMSLN-coated plates (20 µg/mL) in the presence or absence of solMSLN (50 µg/mL), analyzed by flow cytometry (n = 3). **(F)** Cell–cell avidity between linCAR-NK and Capan-2 cells was quantified using acoustic force-based microfluidic microscopy (n = 5). **(G)** Luciferase-based cytotoxicity of lentivirus (LV)-generated CAR($_{LV}$CAR)-NK cells against Capan-2-Luc and SK-OV-3-Luc cells (n = 3). **(H)** Predicted docking model of CLMS10 scFv in complex with matMSLN using Schrödinger software. Residues with side chains within 2.5 Å of the binding interface are highlighted, showing key antigen-antibody interactions. Soluble MSLN regions are indicated in marine blue, and membrane-bound matMSLN in dark blue. Data are

presented as mean ± s.d. Statistical analyses: one-way ANOVA in (C) and two-way ANOVA for (F); two-tailed Student's t-test in (d) and (e); *p < 0.05, **p < 0.01, ***p < 0.001, ****p < 0.0001.

Fig. 4. CAR-MS10 structural optimization and cytokine co-expression enhance CAR-NK cytotoxicity and functionality

(A) Four CAR constructs were designed to evaluate combinations of transmembrane (CD8, NKG2D), costimulatory (4-1BB, OX40, DAP10, and 2B4), and signaling (CD3ζ, DAP12) domains. **(B)** Cytotoxicity of linCAR-NK cells at 12 h and 24 h post co-culture with Capan-2 cells using luciferase-based assay (*n* = 3). **(C)** CD107a degranulation in $CD56^+$ linCAR-NK cells after co-culture with Capan-2 cells, analyzed by flow cytometry (n = 4). **(D)** IFN-γ secretion after 24 h co-culture (*n* = 3). **(E, F)** Metabolic activity [oxygen consumption rate (OCR)] after 2 h stimulation on matMSLN-coated plates (20 μg/mL) (n = 3). **(G)** Intracellular signaling pathway activation by lead construct (linCAR-MS10-OX40ζ), quantified by normalizing the levels of phosphorylated PLCγ and ERK to their respective total forms (n = 3). **(H–J)** Functional assessment of primary NK cells co-transfected with linCAR-MS10-OX40ζ and cytokine-encoding linRNAs (IL2, IL15, or IL21). Luciferase-based cytotoxicity (I) and CD107a degranulation (J) were measured in NK cells co-transfected with single or combined cytokines (n = 3). Data are shown as mean ± s.d. One-way ANOVA was used in panels (B-D), (F), (I), and (J); *p < 0.05, **p < 0.01, ***p < 0.001, ****p < 0.0001.

Fig. 5. circCAR-MS10-CAR-NK cells exhibit prolonged CAR expression, sustained cytotoxicity, and resistance to antigen shedding

(A) Generation of circCAR-NK cells via EP. **(B-D)** CAR expression and viability of linCAR- and circCAR-NK cells over time. **(C)** CAR levels were measured and compared to the EP-negative control (n = 5). **(D)** NK viability was assessed by live/dead staining following EP (n = 3). **(E)** Serial killing assay of CAR-NK cells sequentially exposed to fresh Capan-2 cancer cells at 12 h-intervals. Serial cytotoxicity (F) and IFNγ secretion (I) were evaluated to determine the sustained antitumor activity of circCAR-NK cells (n = 3). (H, I) Impact of solMSLN (50 μg/mL) on CAR-NK cell function during repeated tumor challenges. Serial cancer killing (H) and IFNγ secretion (I) were assessed following solMSLN treatment (50 μg/mL) at each round (n = 3). Data are presented as mean ± s.d. Statistical analyses: one-way ANOVA for (C–G) and two-tailed Student's t-test for (H) and (I); *$p < 0.05$, **$p < 0.01$, ***$p < 0.001$, ****$p < 0.0001$.

Fig. 6. circCAR-MS10-NK cells maintain superior antitumor activity under CAF-induced shedding conditions in vitro and in vivo

(A–B) Soluble MSLN (solMSLN) levels were elevated in Capan-2 cells co-cultured with human pancreatic primary fibroblasts (HPPF) or CAFs (CAF5, CAF6, CAF16, and CAF22), as shown by western blotting; quantified relative to cancer-only controls (n = 3). **(C)** *In vitro* real-time cytotoxicity of circCAR-NK cells co-cultured with mCherry-expressing Capan-2 cancer cells, in the absence or presence of CAFs. CAFs were co-incubated to mimic the tumor microenvironment characterized by shed MSLN secretion. Real time cancer cell death

was assessed by RFP signal analysis (n = 3). **(D)** IHC of MSLN expression in human pancreatic tumor tissues using a CLMS10-derived antibody across stages 1A, 2A, and 4. **(E–F)** In vivo therapeutic effects of CAR-NK cells were evaluated in a metastatic mouse model with intraperitoneal AsPC-1-MSLN-Luc tumors containing CAF6 cells. **(F)** Representative IVIS images of mice treated with mock, linCAR-NK (SS1, 15B6, MS10), circCAR-MS10, or $_{LV}$CAR-MS10 cells (n = 4 per group); all mRNA-CAR groups were co-electroporated with hIL21 mRNA. **(G)** Body weight monitoring during treatment. **(H–I)** Tumor burden quantified via IVIS radiance at day 21 (H) and over time (I) (n = 4). Data are presented as mean ± s.d. Statistical analyses: one-way ANOVA for (B, H) and two-way ANOVA for (C, I); *$p < 0.05$, **$p < 0.01$, ***$p < 0.001$, ****$p < 0.0001$.

PART 1

mRNA-based Rapid CAR screening

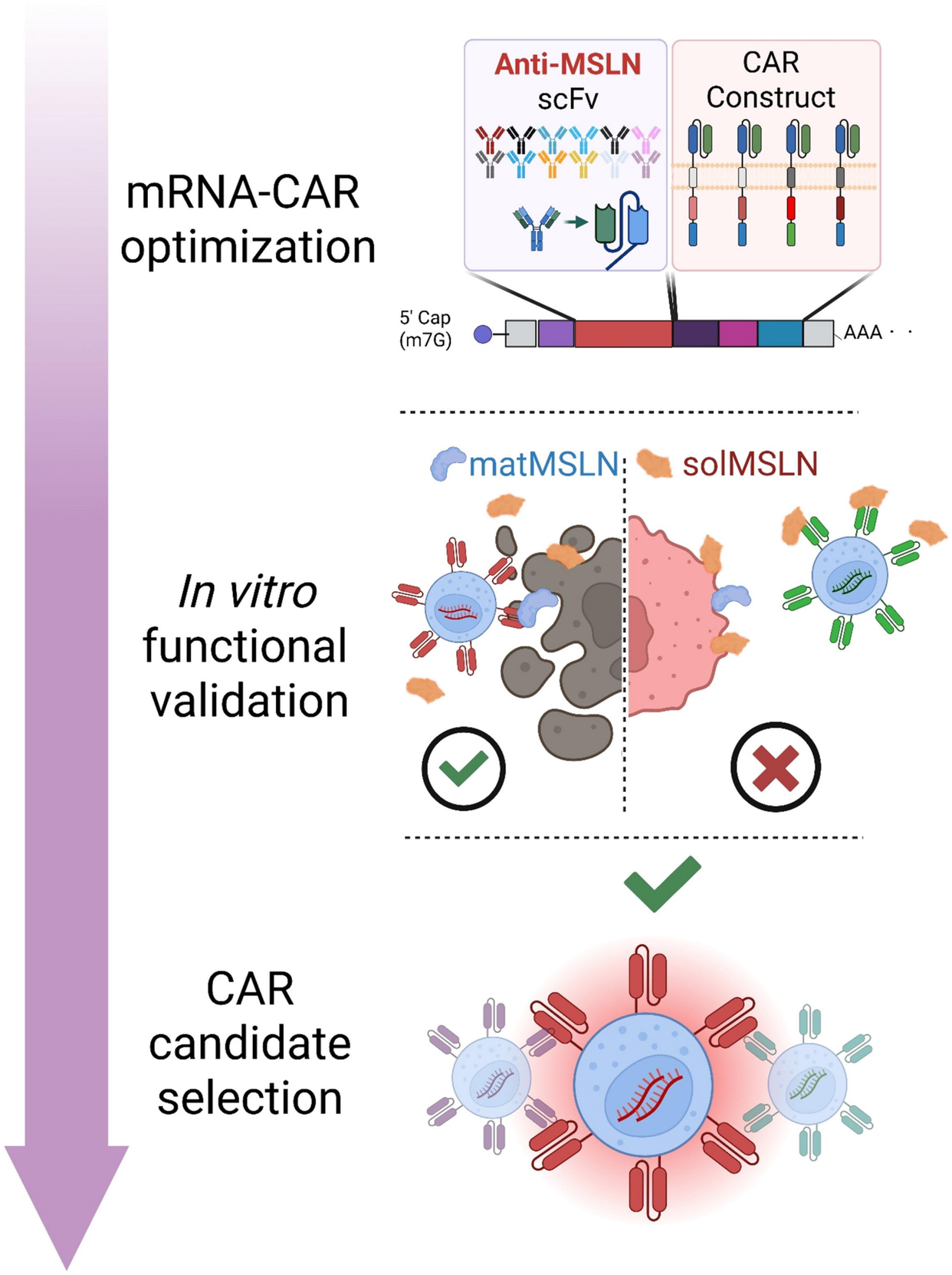

PART 2

Circular RNA for Enhanced CAR-NK Therapy

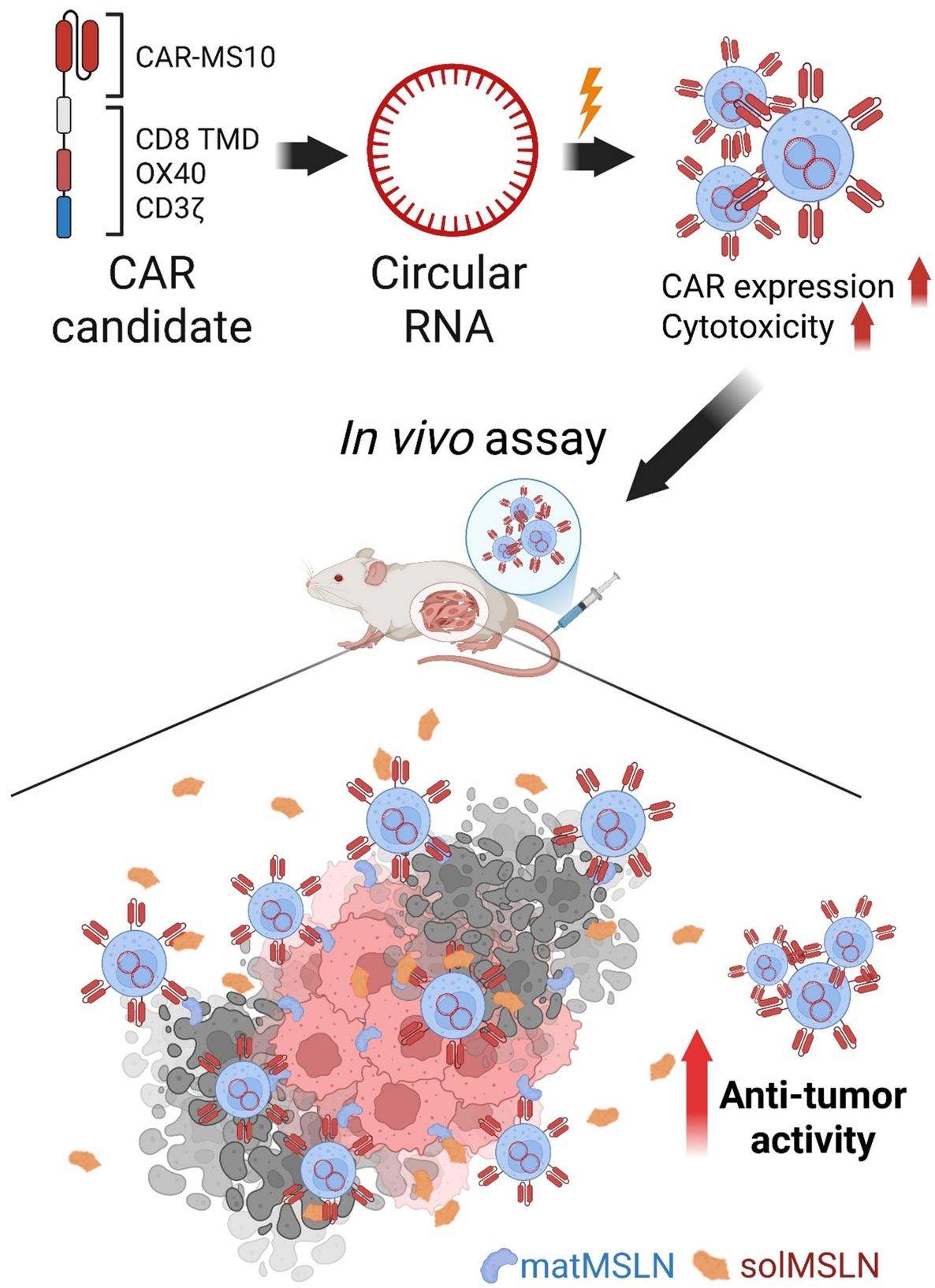

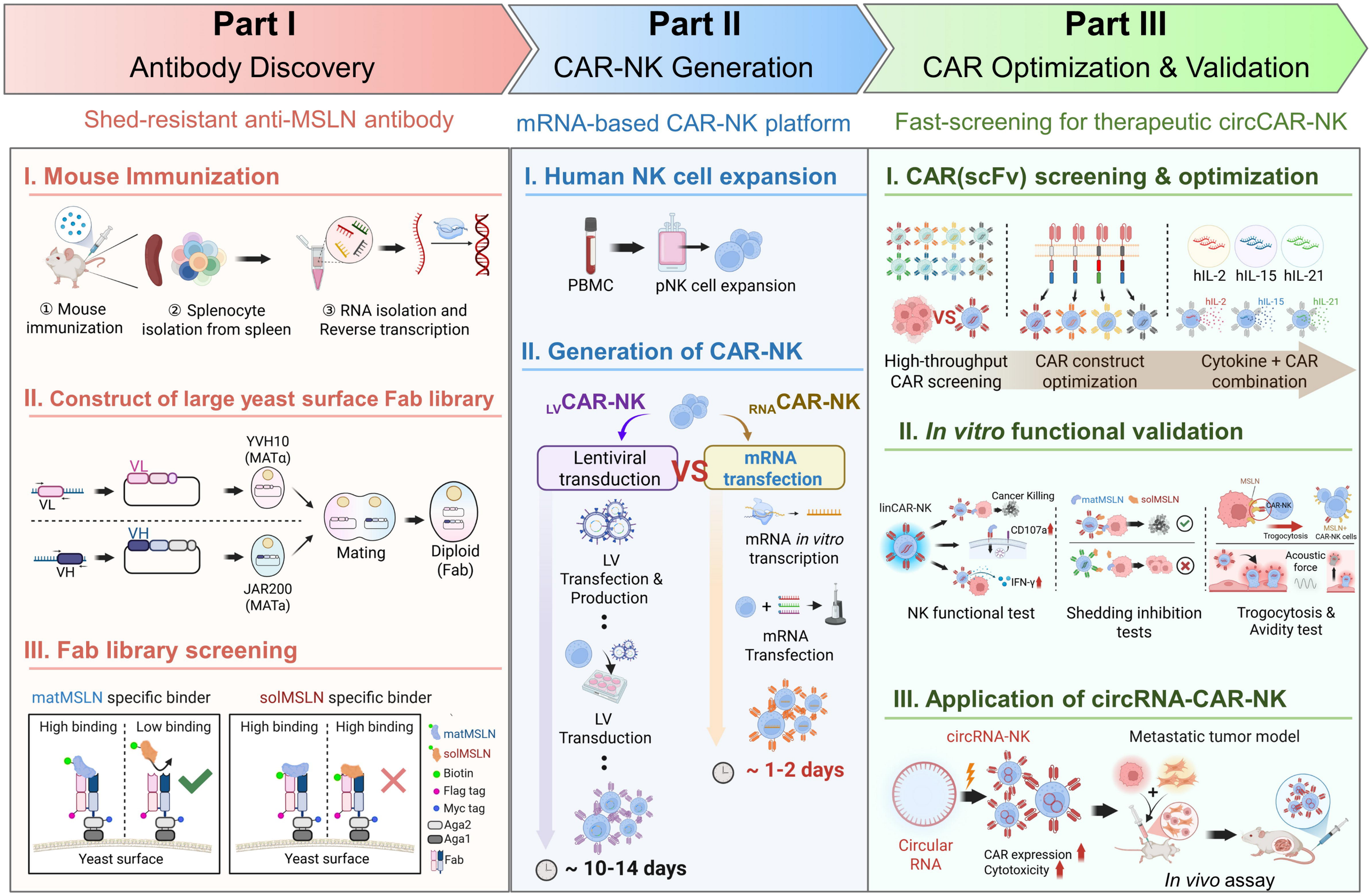
Part I
Antibody Discovery
Part II
CAR-NK Generation
Part III
CAR Optimization & Validation
Shed-resistant anti-MSLN antibody
mRNA-based CAR-NK platform
Fast-screening for therapeutic circCAR-NK
I. Mouse Immunization
① Mouse immunization
② Splenocyte isolation from spleen
③ RNA isolation and Reverse transcription
II. Construct of large yeast surface Fab library
VL
YVH10 (MATα)
VH
JAR200 (MATa)
Mating
Diploid (Fab)
III. Fab library screening
matMSLN specific binder
solMSLN specific binder
High binding
Low binding
High binding
High binding
Yeast surface
Yeast surface
matMSLN
solMSLN
Biotin
Flag tag
Myc tag
Aga2
Aga1
Fab
I. Human NK cell expansion
PBMC
pNK cell expansion
II. Generation of CAR-NK
LvCAR-NK
RNACAR-NK
Lentiviral transduction
VS
mRNA transfection
LV Transfection & Production
LV Transduction
~ 10-14 days
mRNA in vitro transcription
mRNA Transfection
~ 1-2 days
I. CAR(scFv) screening & optimization
hIL-2
hIL-15
hIL-21
VS
High-throughput CAR screening
CAR construct optimization
Cytokine + CAR combination
II. In vitro functional validation
linCAR-NK
Cancer Killing
CD107a
IFN-γ
matMSLN
solMSLN
MSLN
CAR-NK
Trogocytosis
MSLN+ CAR-NK cells
Acoustic force
NK functional test
Shedding inhibition tests
Trogocytosis & Avidity test
III. Application of circRNA-CAR-NK
circRNA-NK
Metastatic tumor model
Circular RNA
CAR expression
Cytotoxicity
In vivo assay

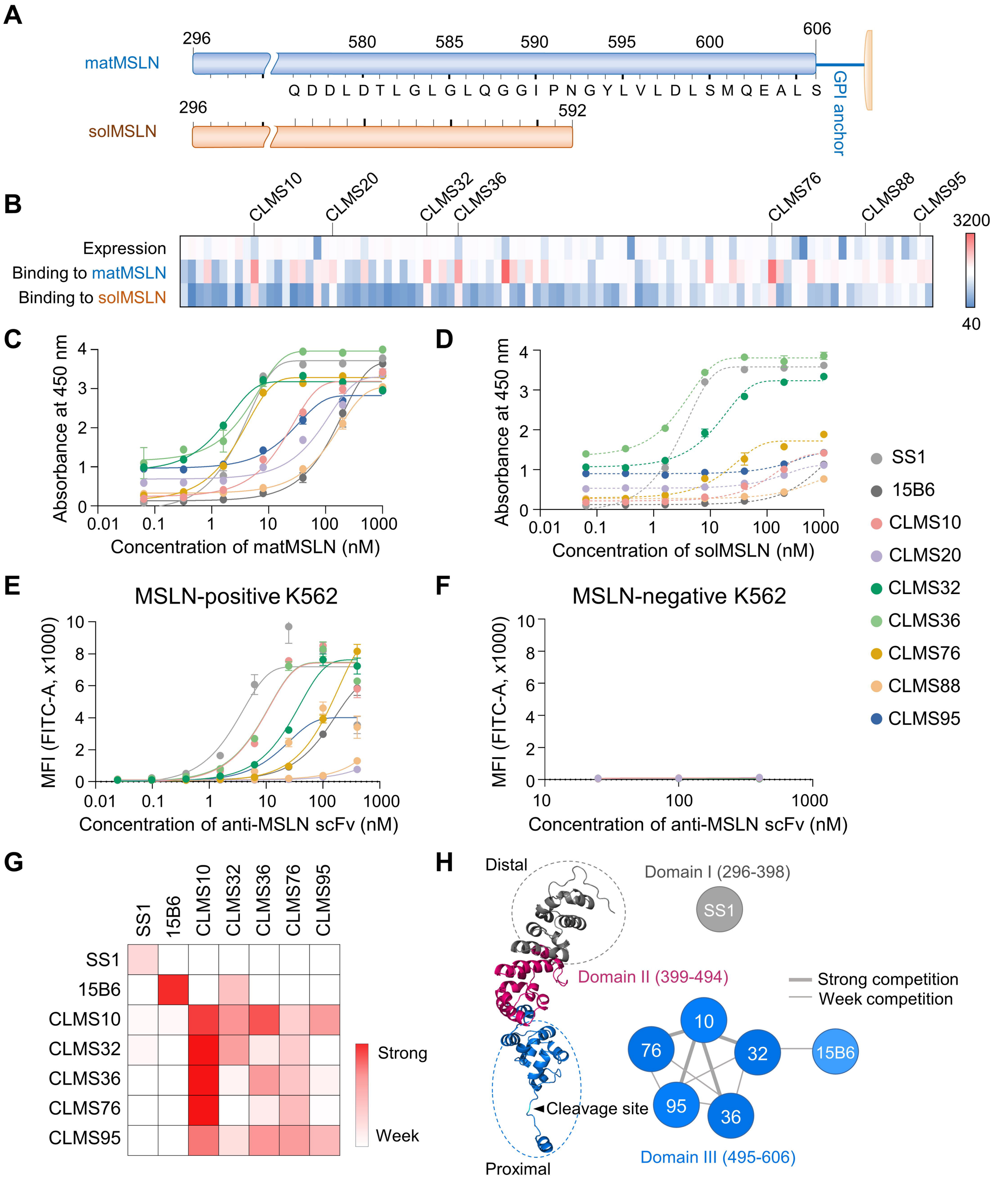
A
matMSLN
296
580
585
590
595
600
606
Q D D L D T L G L G L Q G G I P N G Y L V L D L S M Q E A L S
GPI anchor
solMSLN
296
592
B
CLMS10
CLMS20
CLMS32
CLMS36
CLMS76
CLMS88
CLMS95
Expression
Binding to matMSLN
Binding to solMSLN
3200
40
C
Absorbance at 450 nm
Concentration of matMSLN (nM)
D
Absorbance at 450 nm
Concentration of solMSLN (nM)
SS1
15B6
CLMS10
CLMS20
CLMS32
CLMS36
CLMS76
CLMS88
CLMS95
E
MSLN-positive K562
MFI (FITC-A, x1000)
Concentration of anti-MSLN scFv (nM)
F
MSLN-negative K562
MFI (FITC-A, x1000)
Concentration of anti-MSLN scFv (nM)
G
SS1
15B6
CLMS10
CLMS32
CLMS36
CLMS76
CLMS95
Strong
Week
H
Distal
Domain I (296-398)
SS1
Domain II (399-494)
Strong competition
Week competition
10
76
32
15B6
95
36
Cleavage site
Domain III (495-606)
Proximal

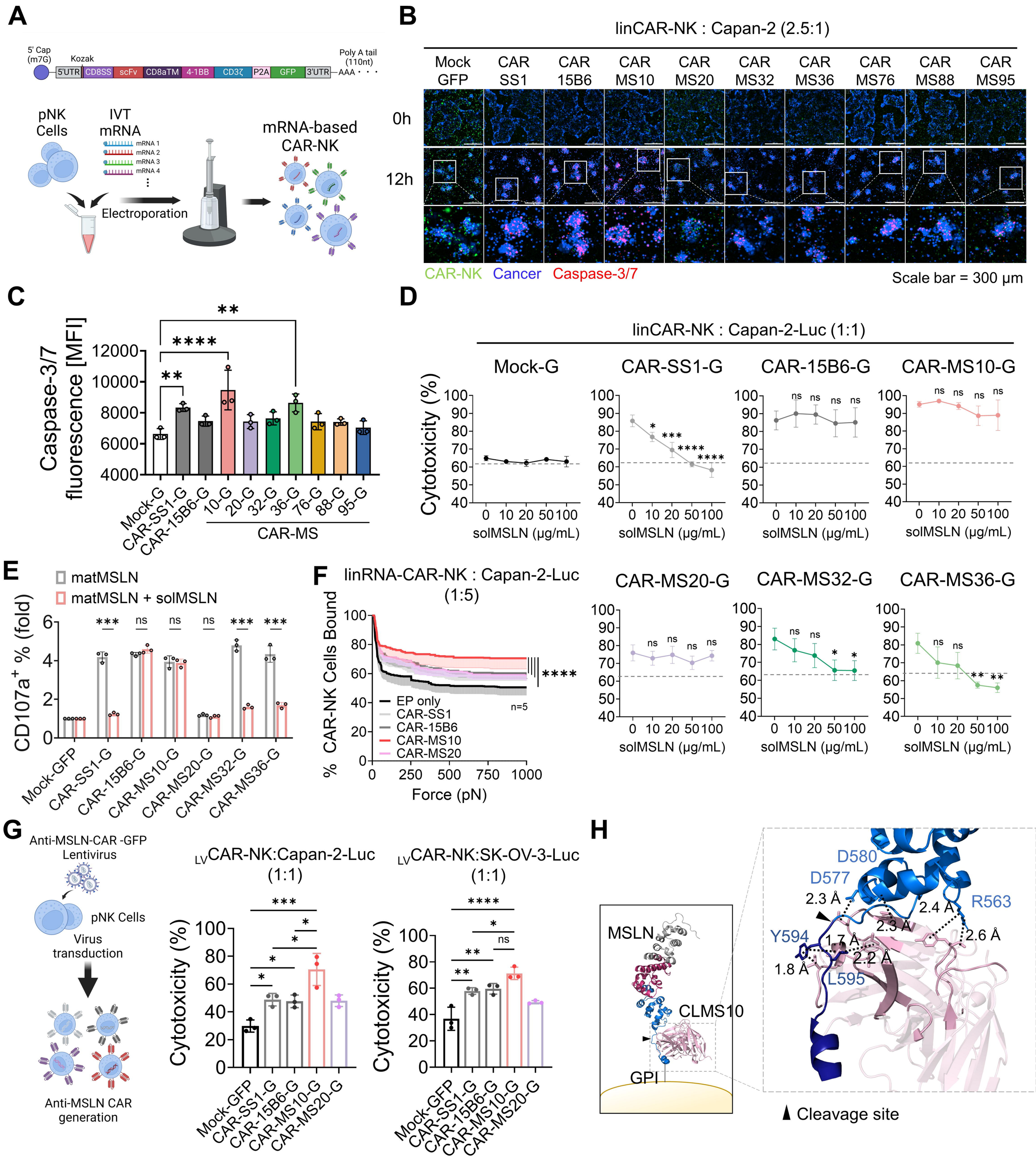
A
5' Cap (m7G)
Kozak
5'UTR
CD8SS
scFv
CD8aTM
4-1BB
CD3ζ
P2A
GFP
3'UTR
Poly A tail (110nt)
AAA
pNK Cells
IVT mRNA
mRNA 1
mRNA 2
mRNA 3
mRNA 4
Electroporation
mRNA-based CAR-NK
B
linCAR-NK : Capan-2 (2.5:1)
Mock GFP
CAR SS1
CAR 15B6
CAR MS10
CAR MS20
CAR MS32
CAR MS36
CAR MS76
CAR MS88
CAR MS95
0h
12h
CAR-NK
Cancer
Caspase-3/7
Scale bar = 300 µm
C
Caspase-3/7 fluorescence [MFI]
12000
10000
8000
6000
4000
**
****
**
Mock-G
CAR-SS1-G
CAR-15B6-G
10-G
20-G
32-G
36-G
76-G
88-G
95-G
CAR-MS
D
linCAR-NK : Capan-2-Luc (1:1)
Mock-G
CAR-SS1-G
CAR-15B6-G
CAR-MS10-G
CAR-MS20-G
CAR-MS32-G
CAR-MS36-G
Cytotoxicity (%)
solMSLN (µg/mL)
ns
E
matMSLN
matMSLN + solMSLN
CD107a+ % (fold)
Mock-GFP
CAR-SS1-G
CAR-15B6-G
CAR-MS10-G
CAR-MS20-G
CAR-MS32-G
CAR-MS36-G
F
linRNA-CAR-NK : Capan-2-Luc (1:5)
% CAR-NK Cells Bound
Force (pN)
EP only
CAR-SS1
CAR-15B6
CAR-MS10
CAR-MS20
n=5
G
Anti-MSLN-CAR -GFP Lentivirus
pNK Cells
Virus transduction
Anti-MSLN CAR generation
LVCAR-NK:Capan-2-Luc (1:1)
LVCAR-NK:SK-OV-3-Luc (1:1)
Cytotoxicity (%)
H
MSLN
CLMS10
GPI
D580
D577
R563
Y594
L595
2.3 Å
2.4 Å
2.3 Å
2.6 Å
1.7 Å
2.2 Å
1.8 Å
Cleavage site

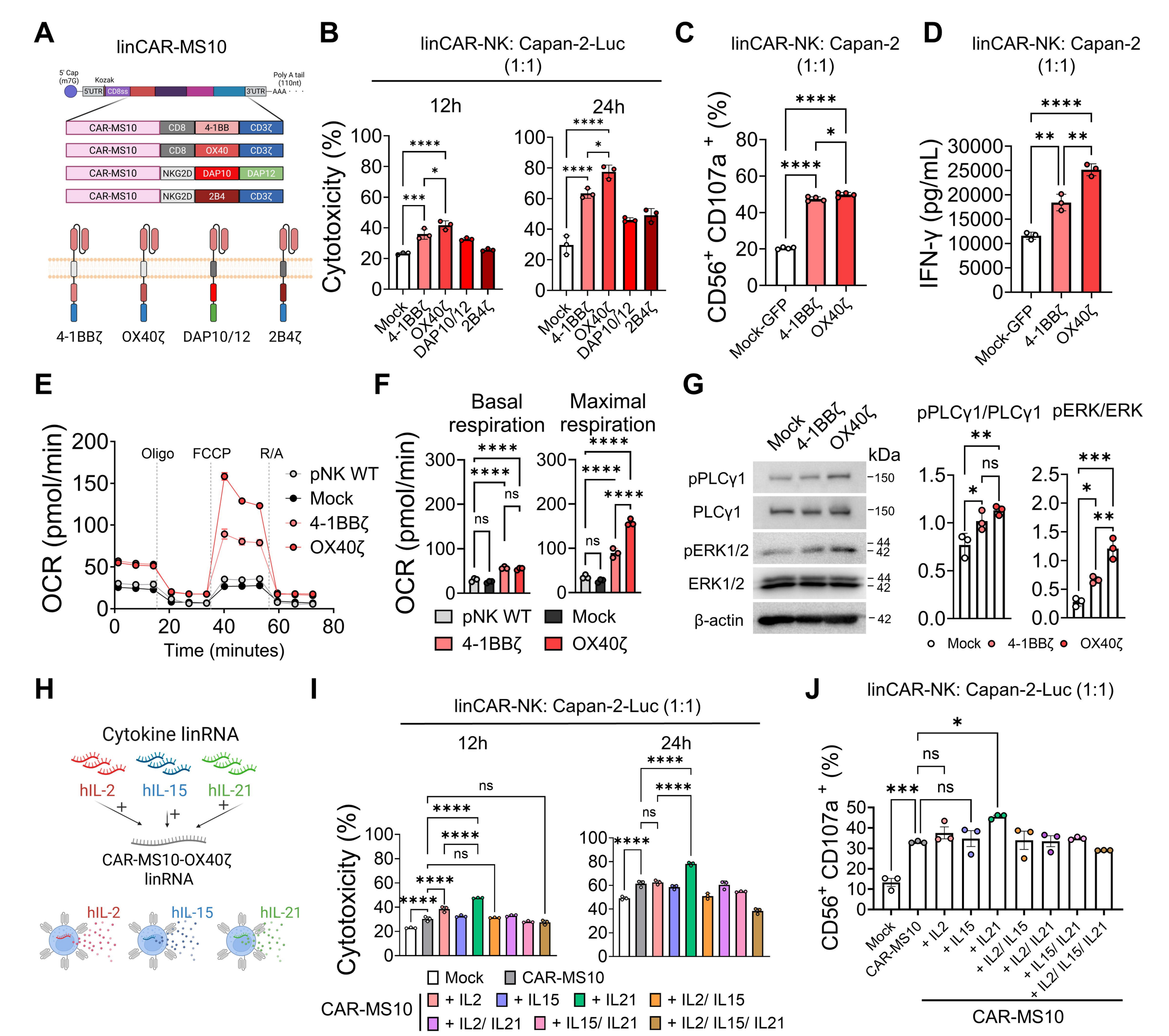
A
linCAR-MS10
5' Cap (m7G)
Kozak
Poly A tail (110nt)
5'UTR
CD8ss
3'UTR
AAA
CAR-MS10 CD8 4-1BB CD3ζ
CAR-MS10 CD8 OX40 CD3ζ
CAR-MS10 NKG2D DAP10 DAP12
CAR-MS10 NKG2D 2B4 CD3ζ
4-1BBζ
OX40ζ
DAP10/12
2B4ζ
B
linCAR-NK: Capan-2-Luc (1:1)
12h
24h
Cytotoxicity (%)
Mock
4-1BBζ
OX40ζ
DAP10/12
2B4ζ
C
linCAR-NK: Capan-2 (1:1)
CD56+ CD107a+ (%)
Mock-GFP
4-1BBζ
OX40ζ
D
linCAR-NK: Capan-2 (1:1)
IFN-γ (pg/mL)
Mock-GFP
4-1BBζ
OX40ζ
E
OCR (pmol/min)
Oligo
FCCP
R/A
pNK WT
Mock
4-1BBζ
OX40ζ
Time (minutes)
F
Basal respiration
Maximal respiration
OCR (pmol/min)
pNK WT
Mock
4-1BBζ
OX40ζ
G
Mock
4-1BBζ
OX40ζ
kDa
pPLCγ1
PLCγ1
pERK1/2
ERK1/2
β-actin
pPLCγ1/PLCγ1
pERK/ERK
Mock
4-1BBζ
OX40ζ
H
Cytokine linRNA
hIL-2
hIL-15
hIL-21
CAR-MS10-OX40ζ linRNA
hIL-2
hIL-15
hIL-21
I
linCAR-NK: Capan-2-Luc (1:1)
12h
24h
Cytotoxicity (%)
Mock
CAR-MS10
CAR-MS10
+ IL2
+ IL15
+ IL21
+ IL2/ IL15
+ IL2/ IL21
+ IL15/ IL21
+ IL2/ IL15/ IL21
J
linCAR-NK: Capan-2-Luc (1:1)
CD56+ CD107a+ (%)
Mock
CAR-MS10
+ IL2
+ IL15
+ IL21
+ IL2/ IL15
+ IL2/ IL21
+ IL15/ IL21
+ IL2/ IL15/ IL21
CAR-MS10

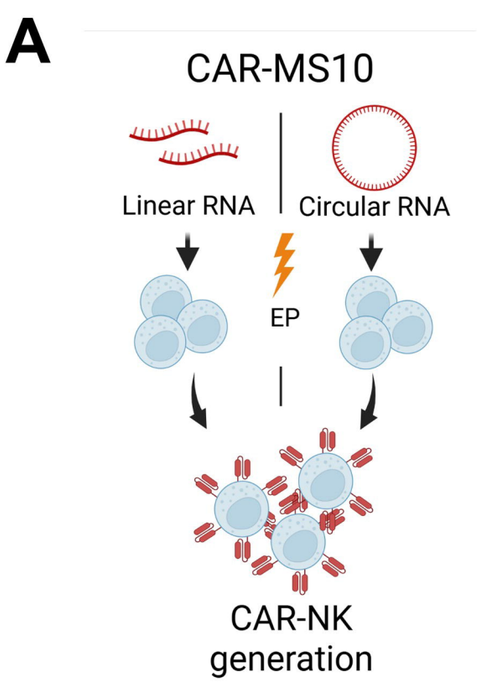
A
CAR-MS10
Linear RNA
Circular RNA
EP
CAR-NK
generation

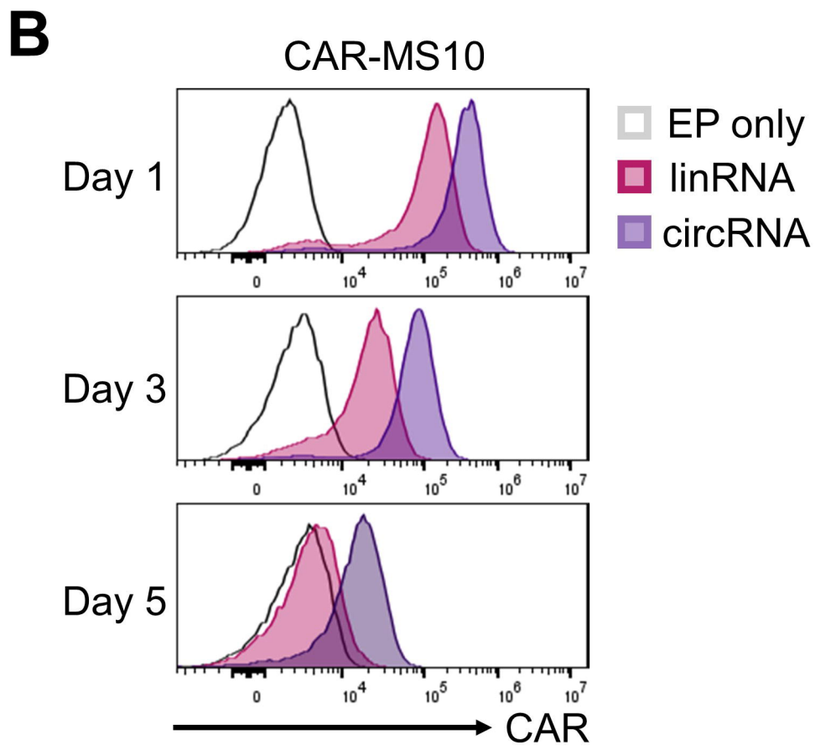
B
CAR-MS10
Day 1
Day 3
Day 5
EP only
linRNA
circRNA
CAR

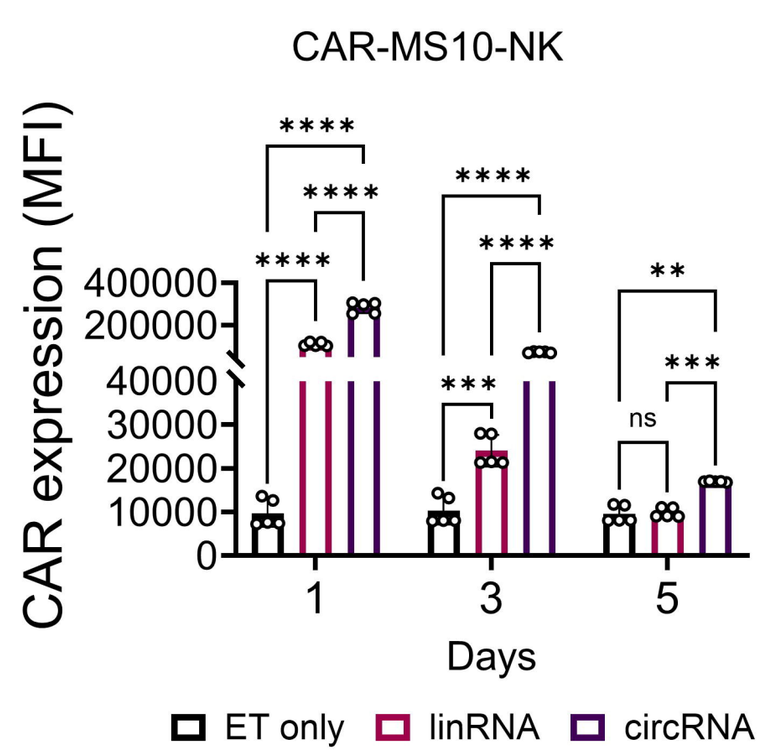
C
CAR-MS10-NK
CAR expression (MFI)
Days
ET only
linRNA
circRNA

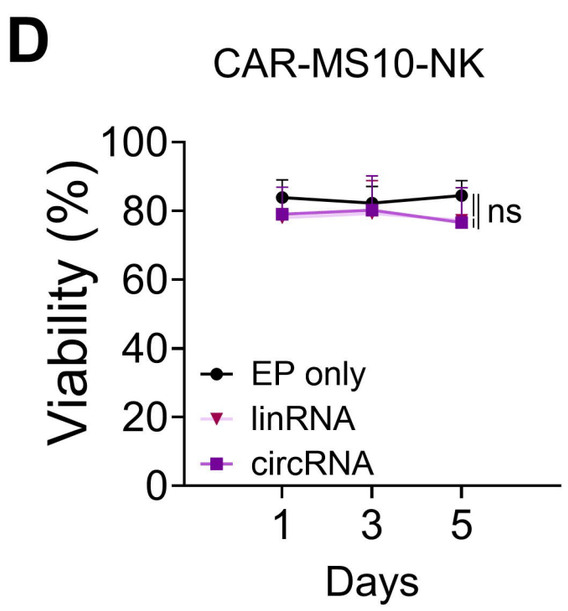
D
CAR-MS10-NK
Viability (%)
ns
EP only
linRNA
circRNA
Days

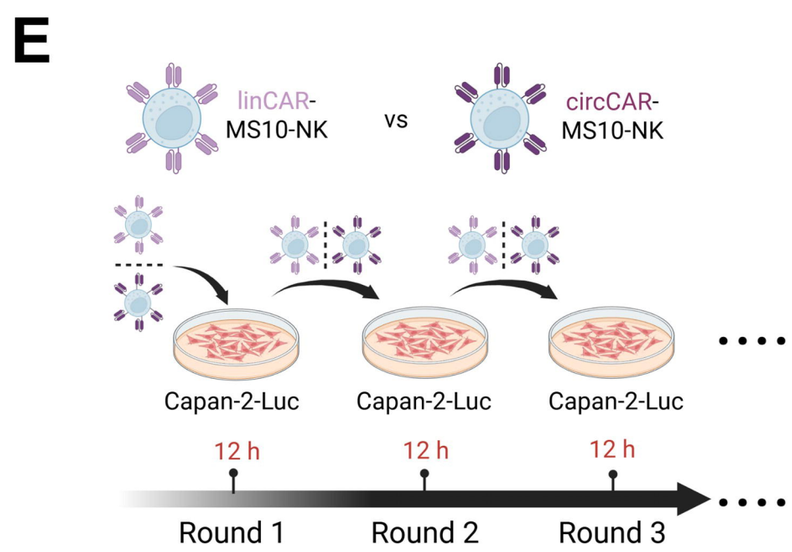
E
linCAR-
MS10-NK
vs
circCAR-
MS10-NK
Capan-2-Luc
Capan-2-Luc
Capan-2-Luc
12 h
12 h
12 h
Round 1
Round 2
Round 3

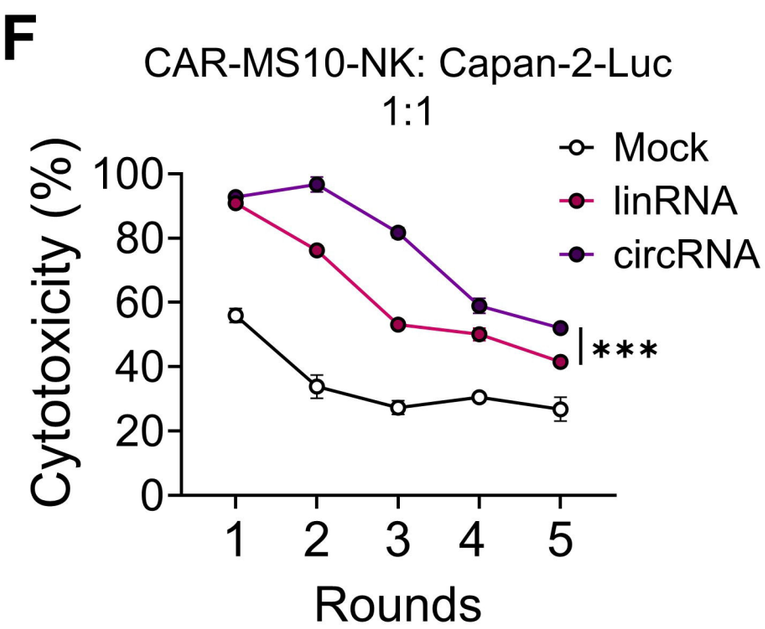
F
CAR-MS10-NK: Capan-2-Luc
1:1
Cytotoxicity (%)
Mock
linRNA
circRNA
Rounds

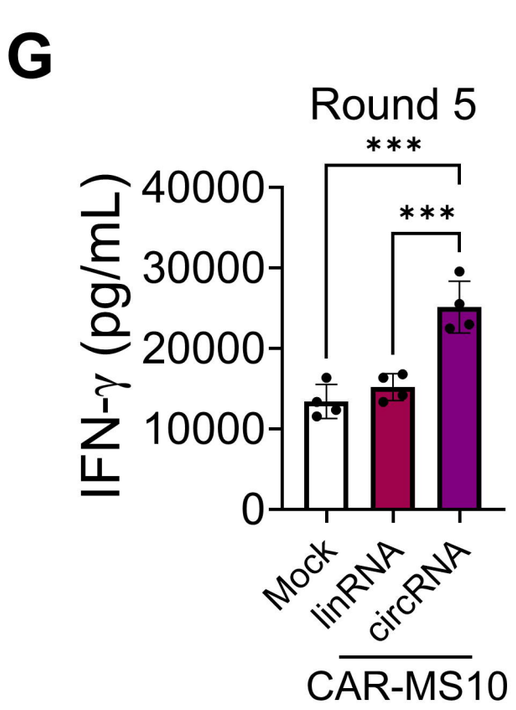
G
Round 5
IFN-γ (pg/mL)
Mock
linRNA
circRNA
CAR-MS10

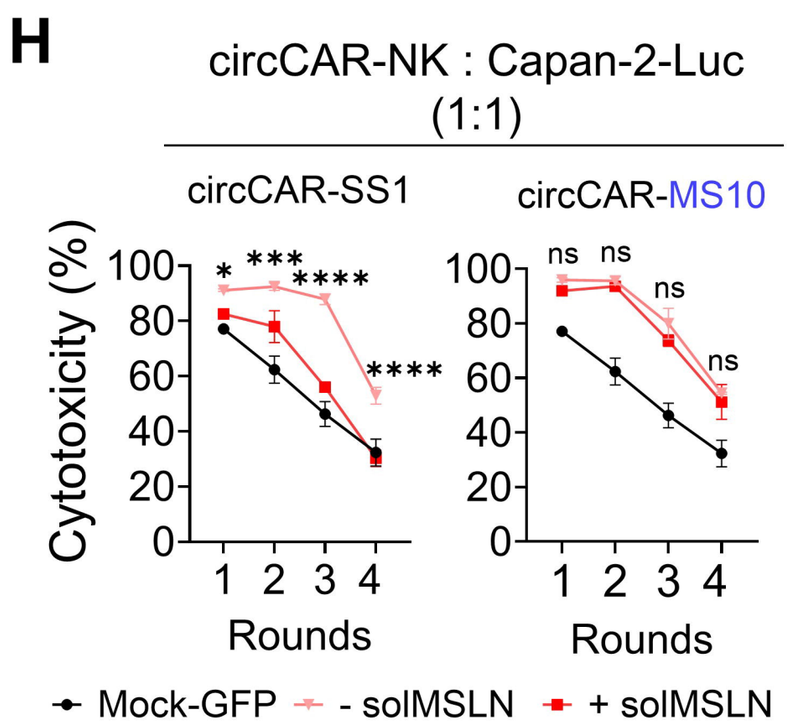
H
circCAR-NK : Capan-2-Luc
(1:1)
circCAR-SS1
circCAR-MS10
Cytotoxicity (%)
Rounds
Mock-GFP
- solMSLN
+ solMSLN

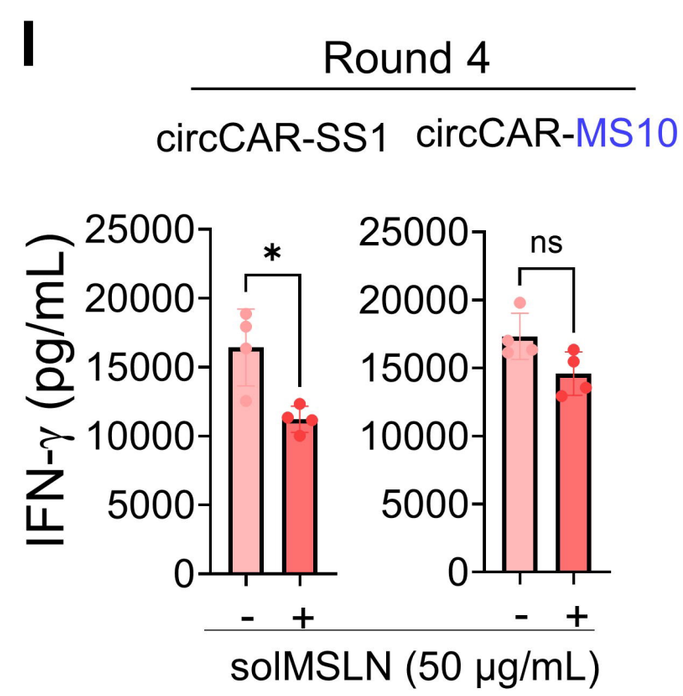
I
Round 4
circCAR-SS1
circCAR-MS10
IFN-γ (pg/mL)
solMSLN (50 μg/mL)

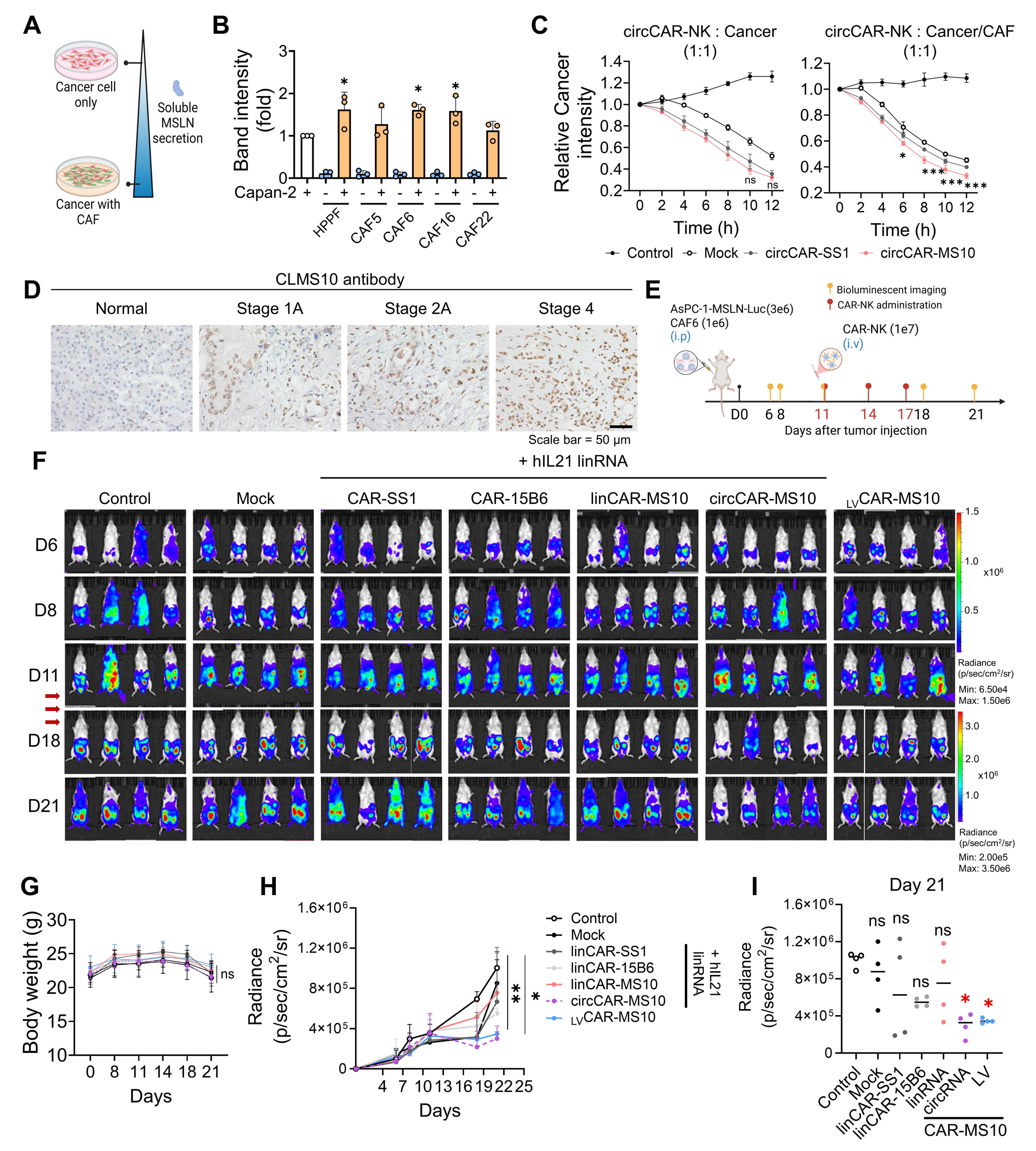
A
Cancer cell only
Soluble MSLN secretion
Cancer with CAF
B
Band intensity (fold)
Capan-2
HPPF
CAF5
CAF6
CAF16
CAF22
C
circCAR-NK : Cancer (1:1)
circCAR-NK : Cancer/CAF (1:1)
Relative Cancer intensity
Time (h)
Control
Mock
circCAR-SS1
circCAR-MS10
D
CLMS10 antibody
Normal
Stage 1A
Stage 2A
Stage 4
Scale bar = 50 μm
E
Bioluminescent imaging
CAR-NK administration
AsPC-1-MSLN-Luc(3e6)
CAF6 (1e6)
(i.p)
CAR-NK (1e7)
(i.v)
D0
Days after tumor injection
F
+ hIL21 linRNA
Control
Mock
CAR-SS1
CAR-15B6
linCAR-MS10
circCAR-MS10
LVCAR-MS10
D6
D8
D11
D18
D21
Radiance (p/sec/cm²/sr)
Min: 6.50e4
Max: 1.50e6
Min: 2.00e5
Max: 3.50e6
G
Body weight (g)
Days
H
Radiance (p/sec/cm²/sr)
Days
linRNA
+ hIL21
I
Day 21
Radiance (p/sec/cm²/sr)
Control
Mock
linCAR-SS1
linCAR-15B6
linRNA
circRNA
LV
CAR-MS10